

# MOMENTS, TIME-INVERSION AND SOURCE IDENTIFICATION FOR THE HEAT EQUATION

KANG LIU<sup>1</sup> AND ENRIQUE ZUAZUA<sup>234</sup>

**ABSTRACT.** We address the initial source identification problem for the heat equation, a notably ill-posed inverse problem characterized by exponential instability. Departing from classical Tikhonov regularization, we propose a novel approach based on moment analysis of the heat flow, transforming the problem into a more stable inverse moment formulation. By evolving the measured terminal time moments backward through their governing ODE system, we recover the moments of the initial distribution. We then reconstruct the source by solving a convex optimization problem that minimizes the total variation of a measure subject to these moment constraints. This formulation naturally promotes sparsity, yielding atomic solutions that are sums of Dirac measures. Compared to existing methods, our moment-based approach reduces exponential error growth to polynomial growth with respect to the terminal time. We provide explicit error estimates on the recovered initial distributions in terms of moment order, terminal time, and measurement errors. In addition, we develop efficient numerical discretization schemes and demonstrate significant stability improvements of our approach through comprehensive numerical experiments.

## 1. INTRODUCTION

**1.1. Problem statement and motivation.** Let us consider the heat equation in  $\mathbb{R}^d$  with  $d \in \mathbb{Z}_+$ :

$$(1.1) \quad \begin{cases} \partial_t u(x, t) - \Delta u(x, t) = 0, & \text{for } (x, t) \in \mathbb{R}^d \times \mathbb{R}_+, \\ u(\cdot, 0) = u_0^*, \end{cases}$$

where  $u_0^*$  lies in the tempered distribution space  $\mathcal{S}'(\mathbb{R}^d)$ . Fix a terminal time  $T > 0$ .

The **time-inversion** or **initial source identification problem** associated with equation (1.1) is to determine the initial condition  $u_0^*$  from the observed terminal solution  $u(\cdot, T)$ . This inverse problem has significant real-world applications, particularly in detecting pollution sources [14, 20, 28] and in image denoising [15].

---

<sup>1</sup>UNIVERSITÉ BOURGOGNE EUROPE, CNRS, INSTITUT DE MATHÉMATIQUES DE BOURGOGNE, 21000 DIJON, FRANCE.

<sup>2</sup>FRIEDRICH - ALEXANDER - UNIVERSITÄT ERLANGEN - NÜRNBERG, DEPARTMENT OF MATHEMATICS, CHAIR FOR DYNAMICS, CONTROL, MACHINE LEARNING, AND NUMERICS (ALEXANDER VON HUMBOLDT PROFESSORSHIP), 91058 ERLANGEN, GERMANY.

<sup>3</sup>UNIVERSIDAD AUTÓNOMA DE MADRID, DEPARTAMENTO DE MATEMÁTICAS, 28049 MADRID, SPAIN.

<sup>4</sup>CHAIR OF COMPUTATIONAL MATHEMATICS, FUNDACIÓN DEUSTO, 48007 BILBAO, BASQUE COUNTRY, SPAIN.

*E-mail addresses:* kang.liu@u-bourgogne.fr, enrique.zuazua@fau.de.

*Date:* July 4, 2025.

E. Zuazua was funded by the European Research Council (ERC) under the European Union's Horizon 2030 research and innovation programme (grant agreement NO: 101096251-CoDeFeL), the Alexander von Humboldt-Professorship program, the ModConFlex Marie Curie Action, HORIZON-MSCA-2021-dN-01, the COST Action MAT-DYNNET, the Transregio 154 Project of the DFG, AFOSR Proposal 24IOE027 and grants PID2020-112617GB-C22/AEI/10.13039/501100011033 and TED2021131390B-I00/ AEI/10.13039/501100011033 of MINECO (Spain), and Madrid GovernmentUAM Agreement for the Excellence of the University Research Staff in the context of the V PRICIT (Regional Programme of Research and Technological Innovation).

Although the general formulation considers  $u_0^* \in \mathcal{S}'(\mathbb{R}^d)$ , in many practical settings the source is at a finite number of points (e.g. pollution spills, point-heat sources):

$$(1.2) \quad u_0^* = \sum_{i=1}^N m_i \delta_{x_i},$$

with  $m_i \in \mathbb{R}$  and  $x_i \in \mathbb{R}^d$ . This *atomic ansatz* captures the inherent sparsity of the physical sources and, thanks to the density of finite Dirac sums in  $\mathcal{S}'(\mathbb{R}^d)$  (in the weak-\* sense), does not sacrifice generality. Several studies, including [21, 4], focus specifically on this setting and highlight the significant challenges associated with recovering such singular sources. This is due to the well-known dramatic ill-posedness of the backward resolution of the heat equation. Our main result (Theorem 2.2) requires only that  $u_0^*$  be a finitely supported Radon measure, thus encompassing the Dirac sum case (1.2). This broadens the scope of existing results and improves upon the assumptions commonly found in the literature.

*Ill-posedness.* The solution of the heat equation (1.1) is given by the convolution of the heat kernel (denoted by  $G(t)$ , see Eq. (2.8)) and the initial distribution.

A natural approach to the initial source identification problem is to solve the optimization problem

$$(1.3) \quad \inf_{u_0 \in \mathcal{S}'(\mathbb{R}^d)} \|G(T) * u_0 - u_{\text{obs}}\|_{L^2(\mathbb{R}^d)},$$

where  $u_{\text{obs}} \approx u(\cdot, T)$  is the observed terminal distribution (assumed, to fix ideas, to lie in  $L^2(\mathbb{R}^d)$ ). However, it is well known that (1.3) is numerically challenging due to its inherent ill-posedness [15, Sec. 1.5].

To illustrate the ill-posedness from a Fourier perspective, assume that (1.3) admits an exact solution  $u_0$  so that

$$G(T) * u_0 = u_{\text{obs}}.$$

Taking the Fourier transform and using the fact that the Fourier transform of  $G(T)$  is  $e^{-T\|\xi\|^2}$ , we deduce that

$$(1.4) \quad \widehat{u}_0(\xi) = e^{T\|\xi\|^2} \widehat{u}_{\text{obs}}(\xi).$$

Since the multiplier  $e^{T\|\xi\|^2}$  grows exponentially with  $\|\xi\|$  and the terminal time  $T$ , even a small perturbation in the observed data  $u_{\text{obs}}$  is greatly amplified when reconstructing  $u_0^*$ . This exponential amplification of high-frequency errors demonstrates the ill-posedness of (1.3).

*Existing methods.* To address this ill-posedness, the classical approach is Tikhonov regularization [30], a technique that stabilizes the solution by penalizing its high-frequency components. By adding a penalty term to (1.3), Tikhonov regularization balances the fidelity to the observations with the regularity of the solution. For the regularization term, typical choices include the  $L^1$  and  $L^2$  norms of  $u_0$ ; see, for example, [21, 4]. However, these penalties directly constrain the solution  $u_0$  to regular functional spaces, such as  $L^1(\mathbb{R}^d)$  and  $L^2(\mathbb{R}^d)$ , making them inadequate for recovering atomic measures. To reconstruct solutions of the form (1.2), a more suitable regularization is the total variation (TV) of  $u_0$ ; see [8]. Nevertheless, such approaches remain highly sensitive to the inherent ill-posedness of the backward heat equation, and their performance degrades significantly as the time horizon  $T$  increases.

This motivates the development of the new moment method we present in this article. As we shall mitigate the impact of ill-posedness significantly.

**1.2. Moment method.** We replace the heat equation with a surrogate dynamically stable system, that preserves the essence of the evolutionary behavior of the original model while enabling more robust inversion.

We consider the dynamics of the moments of  $u(\cdot, t)$ , defined by

$$M_\alpha(t) = \int_{\mathbb{R}^d} x^\alpha u(x, t) dx, \quad \text{for } t > 0,$$

where  $\alpha = (\alpha_1, \dots, \alpha_d) \in \mathbb{Z}_+^d$  and  $x^\alpha = x_1^{\alpha_1} \cdots x_d^{\alpha_d}$ . In [12], the authors show that for different initial distributions sharing the same moments up to a finite order, the difference between the corresponding solutions to (1.1) decays faster (as  $t \rightarrow \infty$ ) than the individual solutions themselves.

Motivated by this result, we propose to recover  $u_0^*$  from the moments of the terminal distribution.

Fix  $k \in \mathbb{Z}_+$ , the order of the moments under consideration. Given observations  $y_\alpha \approx M_\alpha(T)$  for all multi-indices  $\alpha$  with  $\|\alpha\|_1 \leq k$ , our goal is to reconstruct an accurate approximation of the initial condition  $u_0^*$ . The effective means of numerically observing  $y_\alpha$  are presented later in the next subsection.

To implement this methodology, we propose a natural two-step strategy to reconstruct the unknown initial condition  $u_0^*$  – an accurate approximation in practice – from the given measurements  $\{y_\alpha\}_{\|\alpha\|_1 \leq k}$ :

- (1) **Moment Estimation:** Compute the initial moments  $\{M_\alpha(0)\}_{\|\alpha\|_1 \leq k}$  from the terminal observations  $\{y_\alpha\}_{\|\alpha\|_1 \leq k}$ :

$$M_\alpha(T) \approx y_\alpha \quad \Rightarrow \quad M_\alpha(0),$$

by inverting the dynamics of the moments.

- (2) **Initial Condition Reconstruction:** Recover the atomic initial datum  $u_0^*$  from the estimated moments  $\{M_\alpha(0)\}$ :

$$\{M_\alpha(0)\} \quad \Rightarrow \quad u_0 \approx u_0^*,$$

through a convex optimization problem.

In the following paragraphs, we detail these two main steps of the methodology and highlight their advantages over direct approaches to the original inverse problem.

*Inverting the dynamics of the moments.* The moments  $M(t) = (M_\alpha(t))_{\|\alpha\|_1 \leq k}$  satisfy a finite-dimensional system of linear ordinary differential equations (ODE) driven by a constant coefficient matrix  $A$  of dimension  $\binom{k+d}{d} \times \binom{k+d}{d}$ . To simplify the notation, we will omit the index  $k$  in the notation of  $A$ . Of course,  $\binom{k+d}{d}$  coincides with the number of moments corresponding to  $\|\alpha\|_1 \leq k$ .

More precisely, let  $e_i$  denote the  $i$ -th canonical basis vector of  $\mathbb{R}^d$ . Then, the ODE governing  $M(t)$  is given by (for a more rigorous formulation, see Lemma 2.5):

$$(1.5) \quad \frac{dM(t)}{dt} = A M(t), \quad \text{where } A_{\alpha, \alpha'} = \begin{cases} \alpha_i(\alpha_i - 1), & \text{if } \alpha' = \alpha - 2e_i, \\ 0, & \text{otherwise.} \end{cases}$$

An important property of the matrix  $A$ , which is independent of the specific moments of the data under consideration and only depends on its dimension, which depends on  $k$ , is that it is *nilpotent* (see Lemma 2.6), namely:

$$A^{\lfloor k/2 \rfloor + 1} = 0.$$

As a consequence, this leads to a polynomial dynamics fulfilling

$$(1.6) \quad \|M(0)\|_\infty \leq \|M(T)\|_\infty \sum_{i=1}^{\lfloor k/2 \rfloor} c_i T^i,$$

for some constants  $c_i$  independent of  $T$  and only depending on  $A$ . Here and in the sequel  $\|\cdot\|_\infty$  stands for the induced matrix norm on  $\ell^\infty$ . We refer to Lemma 2.6 for the precise formula of the constants  $c_i$ .

Comparing (1.6) with (1.4), we observe a fundamental difference in error growth: the moment inversion error grows at most *polynomially* with  $T$ , in contrast to the *exponential* error growth in (1.4). This suggests that backwards solving the ODE system (1.5) may offer significantly greater numerical stability than directly addressing the original problem (1.3).

This is the starting point of our method. But, as mentioned before, a second key step that we describe below, consists of extracting the atomic initial measure out of the recovered moments.

*Recovering initial distribution from its moments.* The reconstructed moments  $\{M_\alpha(0)\}_{|\alpha| \leq k}$  characterize the initial distribution  $u_0$  only up to order  $k$ , leaving the full recovery under-determined, since infinitely many distributions share these moments.

To determine the sparse initial datum (as in (1.2)), we adopt the *minimum total variation principle*: among all distributions matching the given moments, we select the one with minimal total variation norm.

Furthermore, we restrict the support of the initial data under consideration to a compact domain  $\Omega \subseteq \mathbb{R}^d$ , which acts as an a priori estimate of  $\text{supp}(u_0^*)$ . This compactness assumption serves two key purposes:

- It prevents dispersion towards infinity and non-physical solutions with unbounded support;
- It enables the stable numerical discretization.

The resulting optimization problem to recover an efficient approximation of  $u_0^*$  writes

$$(1.7) \quad \inf_{u_0 \in \mathcal{M}(\Omega)} \|u_0\|_{\text{TV}} \quad \text{subject to} \quad \int_{\mathbb{R}^d} x^\alpha d u_0(x) = M_\alpha(0), \quad \text{for } \|\alpha\|_1 \leq k.$$

As mentioned above,  $\Omega$  is a hyper-parameter of this optimization problem, which plays the role of a priori bound for the support of the true initial distribution  $u_0^*$ . By  $\mathcal{M}(\Omega)$  we denote the space of Radon measures on  $\Omega$ .

For the existence of a solution of (1.7), it suffices that  $\Omega$  has non-empty interior (see Theorem 2.1). For quantitative convergence to the true source  $u_0^*$ , we take  $\Omega$  to be a hypercube containing the support of  $u_0^*$  (see Theorem 2.2).

*Overall formulation.* By combining (1.5) with the moment-constrained optimization problem (1.7), we derive the following compact formulation of the moment reconstruction problem: Fix the terminal time  $T$ , observe the moments of the measure solution at time  $T$ , and then solve the optimization problem

$$(P_{\Omega,k}) \quad \inf_{u_0 \in \mathcal{M}(\Omega)} \|u_0\|_{\text{TV}} \quad \text{subject to} \quad \int_{\mathbb{R}^d} x^\alpha d u_0(x) = (e^{-TA} \mathbf{y})_\alpha, \quad \text{for } \|\alpha\|_1 \leq k.$$

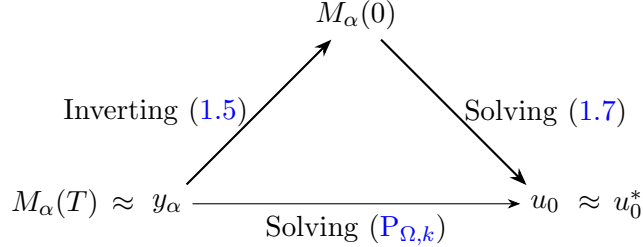
Here,  $A$  is defined in (1.5) and  $\mathbf{y} = (y_\alpha)_{\|\alpha\|_1 \leq k}$  are observations of moments up to order  $k$  at time  $T$ . Problem  $(P_{\Omega,k})$  depends crucially on two key parameters:

- The compact domain  $\Omega \subseteq \mathbb{R}^d$  for support restriction: This parameter is independent of the terminal time  $T$  and the moment order  $k$ . In our main result,  $\Omega$  is fixed as the hypercube  $[-R, R]^d$  aimed to contain the support of  $u_0^*$ . When no prior information about the support is available, one can begin by selecting a sufficiently large  $R$  and gradually decrease  $R$  until a sharp increase on the minimum value of  $(P_{\Omega,k})$  is observed, indicating that the support of  $u_0^*$  has likely been well captured.
- The moment order  $k \in \mathbb{Z}_+$  governing approximation accuracy: The optimal choice of this parameter depends on the observation error; see Remark 2.4 for an explicit asymptotic order. If the error level cannot be determined a priori, one practical strategy is to gradually increase the value of  $k$  starting from  $k = 0$ , and monitor the total variation of the solution.

When a sharp increase occurs, it typically signals that the moment information is no longer reliable beyond that threshold of  $k$ .

Besides the stability benefits discussed earlier, another important advantage of proceeding by solving  $(P_{\Omega,k})$  is that it admits a solution in the form of a finite sum of Dirac measures (1.2); see Theorem 2.1. This follows from classical results known as *Representer Theorems* [16].

The process for tackling  $(P_{\Omega,k})$ , which consists first in inverting (1.5) and then solving (1.7), as described earlier, is shown in the following diagram for clarity.



**1.3. Main results.** Our main contributions to the theoretical analysis of problem  $(P_{\Omega,k})$  are summarized as follows:

- (1) **(Existence of atomic solutions)** In Theorem 2.1 we first establish the existence of an atomic solution to  $(P_{\Omega,k})$  of the form

$$(1.8) \quad u_0^k = \sum_{i=1}^{\binom{k+d}{d}} m_i \delta_{x_i}.$$

by leveraging results from representer theorems.

The number of masses in the sparse atomic reconstruction is exactly the same as the number of moments under consideration.

This existence result holds for any observed data  $\mathbf{y} = (y_{\alpha})_{\|\alpha\|_1 \leq k}$ .

- (2) **(Error estimate)** Next, in Theorem 2.2, assuming that  $u_0^*$  is compactly supported within  $\Omega = [-R, R]^d$ , we establish an error estimate that quantifies the difference between the recovered solution  $u_0^k$  and the true initial distribution  $u_0^*$ . This difference, measured by the Kantorovich distance (see Definition 1.1), is given by:

$$(1.9) \quad \|u_0^k - u_0^*\|_{\text{Kant}} \leq C_1 \left( \frac{\|u_0^*\|_{\text{TV}}}{k} + k^{k/2} e^{C_2 k} \max \left\{ T^{\lfloor k/2 \rfloor}, 1 \right\} \|\epsilon\|_{\infty} \right),$$

where  $C_1$  and  $C_2$  are constants depending only on  $d$  and  $R$ . The variable  $\epsilon = (\epsilon_{\alpha})_{\|\alpha\|_1 \leq k}$  represents the observation error of the moments of  $u(\cdot, T)$ .

The right-hand side of (1.9) decomposes into two distinct components:

- (a) The first term, representing the approximation error in our moment reconstruction, is independent of both the terminal time  $T$  and observation error  $\epsilon$ . It decays with the order  $1/k$ , as the moment order  $k \rightarrow \infty$ .
- (b) The second term reveals a crucial analogy but also an important difference: the maximal moment order  $k$  plays a role similar to the frequency cutoff in Fourier analysis (1.4). But, for fixed  $k$ , this term exhibits only *polynomial growth* in  $T$ , in stark contrast to the *exponential growth* seen in (1.4). This improved stability stems directly from the favorable properties of the moment system (1.6).

Based on points (a)-(b), the optimal moment order  $k^*$  is determined by balancing the two competing terms in the reconstruction error estimate. As detailed in Remark 2.4, if

the observation errors satisfy

$$\delta_1 \leq \|\epsilon\|_\infty \leq \delta_2, \quad \text{for all } k \geq 0,$$

with  $0 < \delta_1 \leq \delta_2 < 1/(2e)$ , then the unique solution  $k^*$  to the balancing condition satisfies the asymptotic bounds

$$(1.10) \quad \frac{c_1 \ln(1/\delta_2)}{\ln T + \ln \ln(1/\delta_2)} \leq k^* \leq \frac{c_2 \ln(1/\delta_1)}{\ln T + \ln \ln(1/\delta_1)},$$

where  $c_1, c_2$  are constants independent of  $\delta_1, \delta_2$ , and  $T$ . This framework captures two relevant regimes:

- If the observation becomes more accurate (i.e.,  $\delta_2 \rightarrow 0$ ) while  $T$  is fixed, then the optimal order  $k^* \rightarrow \infty$ , and the recovery error tends to zero.
- Conversely, if the final time  $T$  increases and the lower bound  $\delta_1$  also grows with  $T$  (as is common in practice due to error accumulation), then  $k^*$  decreases and the reconstruction error increases.

For complete technical details and extended discussion of (1.9), including precise convergence rates, see the full formulation in (2.2) and the analysis in Remarks 2.3 and 2.4.

*Techniques used in the proof.* The proof of our main results combines techniques from several areas, including the representer theorem, optimal transportation, and polynomial approximation.

We apply the representer theorem from [16] to show that the extreme points of the solution set of  $(P_{\Omega,k})$  are sums of Dirac measures. Optimization problems over measures, together with their associated representer theorems, play a fundamental role in classical inverse problems; see [32] and references therein. The core idea behind representer theorems is that the extreme points of the feasible set, defined by linearly independent test functions, take the form of finite sums of Dirac measures. In practice, when the test functions are monomials, this recovers the classical result known as Tchakaloff's Theorem [2].

Notably, problem  $(P_{\Omega,k})$  also bears strong resemblance to mean-field relaxation problems arising in the training of neural networks [11, 23, 22]. The use of representer theorems in such machine learning settings has recently drawn increasing attention; see, for example, [1, 31, 22].

To quantify the distance between the solution of  $(P_{\Omega,k})$  and the true initial distribution  $u_0^*$ , we use the Kantorovich distance, as introduced in [19, 29], which is also referred to as the flat metric in the literature. This metric generalizes the Wasserstein distance [33, Sec. 6] from probability measures to signed measures. We discuss the connection between the Kantorovich and Wasserstein distances in Section 2.4. A key feature of the Kantorovich distance is that it is defined via duality with respect to test functions that are 1-Lipschitz continuous, i.e., there exists  $v^*$ , with  $\|v^*\|_{C(\Omega)} \leq 1$  and  $\text{Lip}(v^*) \leq 1$ , such that

$$\|u_0^k - u_0^*\|_{\text{Kant}} = \int_{\Omega} v^* d(u_0^k - u_0^*).$$

The test function  $v^*$  can be approximated by a degree- $k$  polynomial  $p^k$  with an explicit convergence rate of  $1/k$ , as guaranteed by Jackson's Theorem [24]. This allows us to decompose the integral into the sum of two terms:

- (1) First term:  $\int_{\Omega} (v^* - p^k) d(u_0^k - u_0^*)$ . Since the integrand is uniformly bounded by  $C/k$ , it suffices to estimate the total variation of  $u_0^k - u_0^*$ , which is controlled via Lemma 2.7.
- (2) Second term:  $\int_{\Omega} p^k d(u_0^k - u_0^*)$ . Since  $p^k$  is a polynomial of degree  $k$ , its integral against  $u_0^k - u_0^*$  depends on two components: the coefficients of  $p^k$  and the difference between the moments of  $u_0^k$  and  $u_0^*$  up to order  $k$ . The moment differences are controlled by the backward stability of the moment system; see (1.6). The coefficients of  $p^k$  are in turn governed by its  $L^\infty$ -norm in  $\Omega$ , via Bernstein's inequality; see Lemma 5.5.

**1.4. Numerical implementation.** According to the error estimate (1.9), the success of our moment method relies on two main factors: (1) the robust observation of moments, and (2) the accurate resolution of the moment problem  $(P_{\Omega,k})$ . However, each factor poses its own numerical challenge:

- (1) The moment  $M_\alpha(T)$  is not directly accessible through observations. In practice, we can only measure the values of  $u(x, T)$  at a finite set of sensor locations.
- (2) Although  $(P_{\Omega,k})$  is a convex optimization problem, it is posed in the infinite-dimensional Banach space  $\mathcal{M}(\Omega)$ , making the direct application of standard optimization algorithms infeasible.

We address these two challenges in the following paragraphs.

*Observation of moments.* For the numerical computation of  $M_\alpha(T)$ , we adopt quadrature methods. In practice, the values of  $u(\cdot, T)$  are observed through sensors. The position of these sensors can be interpreted as quadrature points for estimating the moments.

We then approximate  $M_\alpha(T)$  by a weighted sum of these observed values, that is,

$$M_\alpha(T) \approx y_\alpha = \sum_{j=1}^n w_j z_j^\alpha u(z_j, T),$$

where  $n$  is the number of sensors, and  $(z_j, w_j)$  denote the sensor positions and corresponding weights. In Section 3.1, we discuss two quadrature methods particularly suited to the approximation of heat moments: (1) uniform quadrature and (2) Gauss–Hermite quadrature. In the uniform case, the sensor positions are independent of  $T$ , whereas in the Gauss–Hermite case, they grow proportionally to  $\sqrt{T}$ .

For a fixed number of sensors, the Gauss–Hermite method achieves better quadrature performance. This superiority becomes more pronounced as  $T$  increases, as illustrated in Figure 2.

*First Discretize, then Optimize.* To solve  $(P_{\Omega,k})$  numerically, we adopt a discretize–then–optimize strategy. Specifically, we discretize the domain  $\Omega$  by selecting  $N$  points:

$$\Omega \xrightarrow{\text{discretize}} \Omega_h = \{x_1, \dots, x_N\}.$$

Then, in  $(P_{\Omega,k})$  we replace  $\mathcal{M}(\Omega)$  with  $\mathcal{M}(\Omega_h)$ , which yields a convex optimization problem in  $\mathbb{R}^N$ :

$$(P_{\Omega,k}^{\text{dis}}) \quad \inf_{\mathbf{m} \in \mathbb{R}^N} \|\mathbf{m}\|_{\ell^1} \quad \text{subject to} \quad B \mathbf{m} = e^{-TA} \mathbf{y},$$

where  $B$  is a (rectangular) Vandermonde matrix with entries

$$b_{\alpha,i} = x_i^\alpha, \quad \text{for } \|\alpha\|_1 \leq k, \quad i = 1, \dots, N.$$

Under mild assumptions on the mesh  $\Omega_h$ , in Lemma 3.1 we prove the existence of solutions of  $(P_{\Omega,k}^{\text{dis}})$ . We can then apply the *Simplex method* [3, Sec. 3] to solve  $(P_{\Omega,k}^{\text{dis}})$ , which returns a solution of the form (1.8) in a finite number of iterations, see Proposition 3.2.

Numerical experiments in Section 4 demonstrate that the solutions of  $(P_{\Omega,k}^{\text{dis}})$ , obtained using our numerical schemes, converge rapidly to the initial source as  $k$  increases. Moreover, the moment method exhibits strong numerical stability even for moderately large values of  $T$ , such as  $T \in [1, 100]$ , significantly outperforming classical algorithms in this regard, as we discuss in more detail below.

Finally, we mention the limitations of moment methods in high-dimensional settings: (1) fixing the maximal moment-order  $k$ , the theoretical error grows exponentially with the dimension  $d$ , as shown in (2.2), and (2) the discretization of  $\Omega$  suffers from the curse of dimensionality.

**1.5. Related work.** *Tikhonov regularization methods.* As previously mentioned, Tikhonov regularization is a classical approach to mitigate the ill-posedness of the initial source identification problem. In [4], the authors introduce a combined penalty involving the  $L^1$  and  $L^2$  norms of  $u_0$  in the formulation of (1.3). However, this penalization prevents the solution from being a sum of Dirac measures as in (1.2). To address this limitation, they propose a two-stage method: first, solve the penalized optimization problem; then, detect the local maxima of the solution; and finally, determine the amplitudes of these maxima by solving a finite-dimensional convex problem. Although numerically efficient for small terminal times (e.g.,  $T = 0.01$  in [4]), this approach lacks reliable theoretical guarantees of convergence and is unstable for large  $T$ .

In contrast, [8] replaces the  $L^p$  penalty with a TV norm penalty  $\|u_0\|_{\text{TV}}$  for (1.3). The authors analyze the structure of the solution using first-order optimality conditions [8, Thm. 3.1 and Thm. 4.4]. When the minimizers of the adjoint solution are finite, this method recovers a sum of Dirac measures as in (1.2). In our work, such sparsity arises naturally through the representer theorem and the finite observations of moments. The regularization formulations in [8] are highly sensitive to the choice of penalty coefficients, and no efficient numerical algorithms are designed to solve these problems.

A further limitation of these Tikhonov-based methods on (1.3) is their reliance on full knowledge of the terminal solution  $u(\cdot, T)$ , which is unrealistic in practical scenarios where only discrete observations of  $u(x, T)$  at sensor locations are available. Our method addresses this by computing moments through quadrature of these pointwise values. The issue of limited observations is also noted in [21], where the authors adapt the formulation of (1.3) using value residuals at sensor locations and impose an  $L^1$  penalty. They prove convergence with respect to observation error (see [21, Thm. 2.2]), but the result holds only in one spatial dimension, assumes the true initial distribution  $u_0^*$  is a single Dirac measure, and does not explicitly characterize the dependence of the convergence rate on the terminal time  $T$ . Our main result, Theorem 2.2, improves on these limitations by providing an explicit error bound that scales polynomially with  $T$ . In contrast to the fixed small terminal times used in [4] and [21] (both with  $T = 0.01$ ), our method remains stable for terminal times up to  $T = 100$  in two dimensions, offering robust performance across a much broader range of scenarios.

*Algorithms for the discretized problem.* The optimization problem  $(P_{\Omega, k}^{\text{dis}})$  is convex, and a variety of algorithms can be used to solve it. These include Bregman iteration [27] and its variants [18], the Alternating Direction Method of Multipliers (ADMM) [17], and primal-dual methods [9]. Following [10], we rewrite  $(P_{\Omega, k}^{\text{dis}})$  as a linear programming problem. Consequently, a natural and robust approach is to solve the discretized problem  $(P_{\Omega, k}^{\text{dis}})$  using the simplex method. Importantly, the simplex method yields solutions located at extreme points of the feasible set (see [3, Thm. 3.3]), which leads to sparse solutions with fewer support points in the recovered initial distribution.

**1.6. Organization and notations.** In Section 2, we establish the existence of solutions to the optimization problem  $(P_{\Omega, k})$  and analyze their convergence to the true initial condition  $u_0^*$  under appropriate assumptions. Building on these theoretical foundations, Section 3 develops numerical methods for both moment observation and efficient solution of  $(P_{\Omega, k})$ . The effectiveness of our moment-based approach for initial source identification is then demonstrated through numerical experiments in Section 4. Finally, Section 5 collects the technical lemmas required for proving our main results.

*Notations.* We begin by fixing notation:

- For  $x \in \mathbb{R}^n$ ,  $\|x\|_p$  denotes the standard  $\ell^p$ -norm
- $\lfloor a \rfloor$  represents the floor function for  $a \in \mathbb{R}$
- $\binom{n}{m}$  is the binomial coefficient for  $n, m \in \mathbb{N}$

Let  $\Omega \subset \mathbb{R}^d$  be compact. We consider:

- $\mathcal{C}(\Omega)$ : The Banach space of continuous functions on  $\Omega$  equipped with the supremum norm  $\|\cdot\|_{\mathcal{C}(\Omega)}$
- $\mathcal{M}(\Omega)$ : Its dual space, identified with Radon measures on  $\Omega$  having finite total variation.

**Definition 1.1** (Kantorovich Norm [19, 29]). For  $u_0 \in \mathcal{M}(\Omega)$ , the Kantorovich norm is

$$(1.11) \quad \|u_0\|_{\text{Kant}} := \max_{\substack{v \in \mathcal{C}(\Omega) \\ \|v\|_{\mathcal{C}(\Omega)} \leq 1 \\ \text{Lip}(v) \leq 1}} \int_{\Omega} v \, du_0,$$

where  $\text{Lip}(v)$  denotes the Lipschitz constant of  $v$ . The maximum is indeed attained [19, Eq. (4.2)].

In this article, we use the Kantorovich norm to quantify the difference between measures. This choice is motivated by the fact that the recovered initial distribution and the true one may have different total masses, in which case the classical Wasserstein distance is not well-defined. When the total mass is preserved, these two norms are equivalent, leading to an error estimate in the Wasserstein distance, as detailed in Section 2.4.

## 2. MAIN RESULTS

The main results of this article are presented in Section 2.1. In Section 2.2, we analyze the dynamics of moments for solutions to the heat equation; these results serve as preliminary tools for the proof of the main error estimates in Section 2.3. Finally, in Section 2.4, we discuss the error estimates in the Wasserstein sense.

**2.1. Main results.** We first show the existence of the solutions of problem  $(\mathbf{P}_{\Omega,k})$ .

**Theorem 2.1** (Existence). *Assume that  $\Omega$  is compact and has a non-empty interior. Then, for any  $k \in \mathbb{Z}_+$ , any  $T > 0$  and any vector  $\mathbf{y} = (y_{\alpha})_{\|\alpha\|_1 \leq k} \in \mathbb{R}^{\binom{k+d}{d}}$ , the following statements hold:*

- (1) *The solution set of  $(\mathbf{P}_{\Omega,k})$  is non-empty, convex, and compact in the weak-\* topology;*
- (2) *The extreme points of the solution set of  $(\mathbf{P}_{\Omega,k})$  are of the form:*

$$(2.1) \quad u_0^k = \sum_{i=1}^{\binom{k+d}{d}} m_i \delta_{x_i},$$

where  $m_i \in \mathbb{R}$ ,  $x_i \in \Omega$ , and  $\delta_{x_i}$  are Dirac measures.

*Proof.* Since  $\Omega$  has nonempty interior, the monomials  $\{x^{\alpha}\}_{\|\alpha\|_1 \leq 1}$  are linearly independent in  $\mathcal{C}(\Omega)$ . Therefore, the conclusions of Theorem 2.1 follow from the Representer Theorem in [16] (see also Theorem 5.1).  $\square$

Next, we bound the error between the solution of  $(\mathbf{P}_{\Omega,k})$  and the true initial distribution  $u_0^*$  in terms of the moment order  $k$  and the measurement error. To quantify this discrepancy, we use the Kantorovich norm (see Definition 1.1).

**Theorem 2.2** (Error estimate). *Assume  $u_0^*$  is a compactly supported Radon measure in  $\mathbb{R}^d$  with a finite total variation and that  $(u, u_0^*)$  satisfies the heat equation (1.1). Let  $R > 0$  be such that*

$$\text{supp}(u_0^*) \subseteq [-R, R]^d =: \Omega.$$

Fix any  $k \in \mathbb{Z}_+^*$  and let

$$\mathbf{y} = (y_{\alpha})_{\|\alpha\|_1 \leq k} \in \mathbb{R}^d$$

denote the vector of observed moments of  $u(\cdot, T)$ . The observation error is given by

$$\epsilon = (\epsilon_{\alpha})_{\|\alpha\|_1 \leq k}, \quad \text{with} \quad \epsilon_{\alpha} = y_{\alpha} - \int_{\mathbb{R}^d} x^{\alpha} u(x, T) \, dx.$$

Let  $u_0^k$  be any solution of  $(P_{\Omega,k})$ . Then, we have

$$(2.2) \quad \|u_0^k - u_0^*\|_{\text{Kant}} \leq \frac{C_d R \|u_0^*\|_{\text{TV}}}{k} + C_{d,R}(k) \max\{T^{\lfloor k/2 \rfloor}, 1\} \|\epsilon\|_\infty,$$

where  $C_d$  is a constant, depending only on  $d$ , and

$$(2.3) \quad C_{d,R}(k) = \left( \sqrt{\frac{k}{\pi}} + \frac{C_d R}{\sqrt{\pi k}} \right) \exp \left( k \left( 1 + 2d/R + \ln \sqrt{k} \right) \right).$$

*Proof.* The proof is presented in Section 2.3.  $\square$

**Remark 2.3** (Error estimate analysis). The right-hand side of the estimate (2.2) consists of two terms:

$$\frac{C_d R \|u_0^*\|_{\text{TV}}}{k} \quad \text{and} \quad C_{d,R}(k) \max\{T^{\lfloor k/2 \rfloor}, 1\} \|\epsilon\|_\infty.$$

Let us analyze each term:

- (1) The first term is independent of the terminal time  $T$  and the observation error  $\epsilon$ . It decays to zero at a rate of  $1/k$ . Therefore, we represent it as

$$\frac{C_0}{k},$$

where  $C_0$  is a constant independent of  $k$ ,  $T$ , and  $\epsilon$ .

For the second term, recalling the definition of  $C_{d,R}(k)$  from (2.3), we obtain the following leading-order expression:

$$C_1 (T k)^{k/2} e^{C_2 k} \|\epsilon\|_\infty,$$

where  $C_1$  and  $C_2$  are constants independent of  $k$ ,  $T$ , and  $\epsilon$ .

- Fixing  $k$ , we observe that the prefactor of  $\|\epsilon\|_\infty$  grows polynomially with  $T$ , which marks a significant improvement over the classical ill-posedness in time illustrated in (1.4), where the error increases exponentially with time.
- The moment order  $k$  plays a role analogous to the frequency amplitude in the Fourier analysis of the inverse problem for (1.1). For large  $k$ , achieving a small reconstruction error at final time requires increasingly accurate moment observations - that is, a smaller observation error  $\epsilon$ . This reflects the inherent ill-posedness of the backward heat equation in the high-frequency regime.

**Remark 2.4** (Optimal choice of the moment order  $k$ ). Let the final time be  $T > 2$ , and assume that the observation errors for all moments (until infinity) satisfy

$$(2.4) \quad \delta_1 \leq \max_{\alpha \in \mathbb{Z}_+^d} |\epsilon_\alpha| \leq \delta_2, \quad \text{for some } 0 < \delta_1 \leq \delta_2 < 1/(2e).$$

As noted in Remark 2.3, the first term in the convergence estimate (2.2) decays in  $k$ , whereas the second grows. Hence the optimal moment order  $k^*$  is determined by balancing

$$\frac{C_0}{k} = C_1 (T k)^{k/2} e^{C_2 k} \|\epsilon\|_\infty,$$

a transcendental equation in  $k$ . Under the constraint (2.4), its unique solution satisfies the following bounds:

$$(2.5) \quad \frac{c_1 \ln(1/\delta_2)}{\ln T + \ln \ln(1/\delta_2)} \leq k^* \leq \frac{c_2 \ln(1/\delta_1)}{\ln T + \ln \ln(1/\delta_1)},$$

where  $c_1, c_2 > 0$  are constants independent of  $\delta_i$  and  $T$ . Substituting this  $k^*$  back into (2.2) yields

$$(2.6) \quad \|u_0^{k^*} - u_0^*\|_{\text{Kant}} \leq \frac{c_3 (\ln T + \ln \ln(1/\delta_2))}{\ln(1/\delta_2)},$$

for some constant  $c_3$  also independent of  $\delta_i$  and  $T$ . From these estimates, we observe:

- For fixed  $T$ , as the maximal error bound  $\delta_2 \rightarrow 0$ , the optimal order  $k^* \rightarrow \infty$  and the reconstruction error vanishes.
- If  $T$  increases so that the minimal error bound  $\delta_1$  typically grows, then  $k^*$  decreases and the reconstruction error increases, in agreement with the numerical results in Figure 3 (A).

**2.2. The dynamic system of moments.** This subsection is dedicated to a rigorous description of the ODE satisfied by the moments of the solution to the heat equation. This ODE plays an essential role in the proof of Theorem 2.2.

Throughout this subsection, we fix  $\Omega$  as a compact subset of  $\mathbb{R}^d$ . For any initial data  $u_0 \in \mathcal{M}(\Omega)$ , the associated solution  $u$  of the heat equation is given explicitly by:

$$(2.7) \quad u(x, t) = (G(\cdot, t) * u_0)(x), \quad \text{for } (x, t) \in \mathbb{R}^d \times \mathbb{R}_+,$$

where  $G(x, t)$  denotes the heat kernel:

$$(2.8) \quad G(x, t) = \frac{1}{(4\pi t)^{d/2}} \exp\left(-\frac{\|x\|^2}{4t}\right), \quad (x, t) \in \mathbb{R}^d \times \mathbb{R}_+.$$

For any  $\alpha \in \mathbb{Z}_+^d$  and  $t \geq 0$ , define

$$M_\alpha(t) := \begin{cases} \int_{\mathbb{R}^d} x^\alpha u(x, t) dx, & \text{if } t > 0, \\ \int_{\mathbb{R}^d} x^\alpha du_0(x), & \text{if } t = 0. \end{cases}$$

The following holds:

**Lemma 2.5** (The ODE system of moments). *Fix any  $k \in \mathbb{Z}_+$  and let  $M(t) = (M_\alpha(t))_{\|\alpha\|_1 \leq k}$ ,  $t \geq 0$ . Then, we have*

$$(2.9) \quad \begin{cases} \frac{dM(t)}{dt} = A M(t), & \text{for } t > 0, \\ M(0) = \lim_{t \rightarrow 0^+} M(t), \end{cases}$$

with  $A$  as in (1.5).

*Proof.* We proceed in several steps.

**Step 1** For any  $t > 0$ , by the heat equation, we have

$$\frac{dM_\alpha(t)}{dt} = \int_{\mathbb{R}^d} x^\alpha \partial_t u(x, t) dx = \int_{\mathbb{R}^d} x^\alpha \Delta u(x, t) dx.$$

Since  $u(\cdot, t) \in \mathcal{S}(\mathbb{R}^d)$ , applying integration by parts twice, we obtain

$$\int_{\mathbb{R}^d} x^\alpha \Delta u(x, t) dx = \sum_{i=1}^d \alpha_i (\alpha_i - 1) \int_{\mathbb{R}^d} x^{\alpha-2e_i} u(x, t) dx,$$

where  $x^{\alpha-2e_i}$  is set to be zero if  $\alpha_i \leq 1$  for any  $i$ . Therefore, equation (2.9) holds for  $t > 0$ .

**Step 2** (The limit  $t \rightarrow 0^+$ ). For any  $t > 0$ , we have

$$M_\alpha(t) = \int_{\mathbb{R}^d} z^\alpha u(z, t) dz = \int_{\mathbb{R}^d} z^\alpha (G(\cdot, t) * u_0)(z) dz = \int_{\mathbb{R}^d} \int_{\Omega} z^\alpha G(x-z, t) du_0(x) dz.$$

Note that there exists a constant  $C_\alpha > 0$  such that

$$(2.10) \quad \int_{\mathbb{R}^d} |z|^\alpha G(x-z, t) dz \leq C_\alpha (|x|^\alpha + t^{\|\alpha\|_1/2}), \quad \text{for } (x, t) \in \mathbb{R}^d \times (0, +\infty).$$

Indeed, using (2.10) and Fubini's theorem, we can interchange the order of integration in  $M_\alpha(t)$ , yielding

$$M_\alpha(t) = \int_{\Omega} \int_{\mathbb{R}^d} z^\alpha G(x-z, t) dz du_0(x).$$

The inner integral can be computed explicitly:

$$\int_{\mathbb{R}^d} z^\alpha G(x - z, t) dz = \sum_{\substack{\beta \leq \alpha \\ \beta_i \text{ even for all } i}} \binom{\alpha}{\beta} x^{\alpha-\beta} (-1)^{\|\beta\|_1} (2t)^{\|\beta\|_1/2} \prod_{i=1}^d (\beta_i - 1)!!.$$

Taking the limit as  $t \rightarrow 0^+$ , we obtain

$$\lim_{t \rightarrow 0^+} \int_{\mathbb{R}^d} z^\alpha G(x - z, t) dz = x^\alpha, \quad \text{for all } x \in \mathbb{R}^d.$$

By inequality (2.10), the absolute value of the integrand is uniformly integrable with respect to  $u_0$  for  $t \geq 0$  bounded, since  $u_0$  has compact support. Therefore, by Lebesgue's Dominated Convergence Theorem, we conclude that

$$\lim_{t \rightarrow 0^+} M_\alpha(t) = M_\alpha(0).$$

**Step 3** (Proof of (2.10)). Let us rewrite the convolution in (2.10) as

$$\int_{\mathbb{R}^d} |z|^\alpha G(x - z, t) dz = \int_{\mathbb{R}^d} |x - z|^\alpha G(z, t) dz.$$

Decompose the right-hand-side by the following inequality:

$$|x - z|^\alpha \leq 2^{\|\alpha\|_1} (|x|^\alpha + |z|^\alpha).$$

Since the total mass of  $G(\cdot, t)$  is 1, it remains to estimate the second integral involving  $|z|^\alpha$ . By a direct computation, splitting the integral along each coordinate direction, we obtain

$$\int_{\mathbb{R}^d} |z|^\alpha G(z, t) dz = \prod_{i=1}^d \frac{1}{\sqrt{4\pi t}} \int_{\mathbb{R}} |z_i|^{\alpha_i} \exp\left(-\frac{z_i^2}{4t}\right) dz_i = \prod_{i=1}^d \frac{(4t)^{\frac{\alpha_i}{2}}}{\sqrt{\pi}} \Gamma\left(\frac{\alpha_i + 1}{2}\right),$$

where  $\Gamma$  is the Gamma function. This yields the term involving  $t^{\|\alpha\|_1/2}$  in (2.10).  $\square$

**Lemma 2.6** (Growth rate). *The matrix  $A$  defined by (1.5) is  $(\lfloor k/2 \rfloor + 1)$ -nilpotent, i.e.,*

$$(2.11) \quad A^{\lfloor k/2 \rfloor + 1} = 0.$$

As a consequence, the solution  $M(\cdot)$  of (2.9) satisfies the following:

$$(2.12) \quad \|M(0)\|_\infty \leq \|M(t)\|_\infty \sum_{j=0}^{\lfloor k/2 \rfloor} \frac{k^j (k-1)^j}{j!} t^j, \quad \text{for any } t \geq 0.$$

*Proof.* Let  $\mathcal{P}_k(\mathbb{R}^d)$  be the space of polynomials in  $d$  variables of total degree at most  $k$ . For any monomial  $x^\alpha$  with  $\alpha = (\alpha_1, \dots, \alpha_d)$ , we have

$$\Delta x^\alpha = \sum_{i \in I_\alpha} \alpha_i (\alpha_i - 1) x^{\alpha-2e_i}, \quad \text{where } I_\alpha = \{i \in \{1, \dots, d\} \mid \alpha_i \geq 2\}.$$

Thus, if we define a linear operator

$$L : \mathcal{P}_k(\mathbb{R}^d) \rightarrow \mathcal{P}_k(\mathbb{R}^d), \quad L p = \Delta p,$$

its matrix representation in the basis  $\{x^\alpha\}_{\|\alpha\|_1 \leq k}$  is exactly

$$A_{\alpha, \alpha'} = \begin{cases} \alpha_i (\alpha_i - 1), & \text{if } \alpha' = \alpha - 2e_i, \\ 0, & \text{otherwise.} \end{cases}$$

Note that applying  $\Delta$  reduces the total degree of a polynomial by 2. Thus, after applying the Laplacian  $\lfloor k/2 \rfloor + 1$  times, we obtain

$$\Delta^{\lfloor k/2 \rfloor + 1} p = 0, \quad \text{for any } p \in \mathcal{P}_k(\mathbb{R}^d).$$

Since  $A$  is the matrix representation of  $\Delta$ , (2.11) follows

Next, from (2.9) we deduce that

$$M(0) = e^{-tA} M(t), \quad \text{for any } t \geq 0.$$

Hence,

$$\|M(0)\|_\infty \leq \|M(t)\|_\infty \|e^{-tA}\|_\infty.$$

Since  $A$  is  $(\lfloor k/2 \rfloor + 1)$ -nilpotent, we have

$$e^{-tA} = \sum_{j=0}^{\lfloor k/2 \rfloor} \frac{(-A)^j}{j!} t^j, \quad \text{for any } t \geq 0.$$

Moreover, by definition,

$$\| -A \|_\infty = \max_{\|\alpha\|_1 \leq k} \sum_{\alpha'} |A_{\alpha, \alpha'}| = \max_{\|\alpha\|_1 \leq k} \sum_{i=1}^d (\alpha_i(\alpha_i - 1))_+ = k(k-1).$$

Combining these estimates, we obtain the desired inequality (2.12).  $\square$

**Lemma 2.7** (A priori bound). *Let  $\Omega = [-R, R]^d$  for some  $R > 0$ . For any  $k \in \mathbb{Z}_+$  and any vector  $\mathbf{y} = (y_\alpha)_{\|\alpha\|_1 \leq k}$ , let  $u_0^k$  be a solution of  $(\mathbf{P}_{\Omega, k})$ . Then, we have*

$$\|u_0^k\|_{\text{TV}} \leq \|\mathbf{y}\|_\infty \sqrt{\frac{k}{\pi}} \exp \left( k \left( 1 + 2d/R + \ln \sqrt{k} \right) \right) \max \left\{ T^{\lfloor k/2 \rfloor}, 1 \right\}.$$

*Proof.* Let  $u_0^k$  be a solution of  $(\mathbf{P}_{\Omega, k})$ , and let  $u$  be its corresponding heat flow. By Lemma 2.5, the moments of  $u$  satisfy the ODE system (2.9), and their growth rates are controlled by (2.12). Since the moments at time  $T$  are given by  $\{y_\alpha\}_{\|\alpha\|_1 \leq k}$ , it follows from (2.12) that

$$\left| \int_{\mathbb{R}^d} x^\alpha du_0^k(x) \right| \leq \|\mathbf{y}\|_\infty \sum_{j=0}^{\lfloor k/2 \rfloor} \frac{k^j (k-1)^j}{j!} T^j, \quad \text{for any } \|\alpha\|_1 \leq k.$$

By Lemma 5.6, we have

$$\sum_{j=0}^{\lfloor k/2 \rfloor} \frac{k^j (k-1)^j}{j!} T^j \leq \sqrt{\frac{k}{\pi}} \exp \left( k + \frac{k}{2} \ln k \right) \max \left\{ T^{\lfloor k/2 \rfloor}, 1 \right\}.$$

Finally, the conclusion follows from Lemma 5.2 and (5.3), given that  $u_0^k$  solves  $(\mathbf{P}_{\Omega, k})$ .  $\square$

**Remark 2.8.** The argument combines two key ingredients:

- (1) *Backward moment propagation:* We first employ the quantitative estimates for the evolution of moments backward in time.
- (2) *Optimality condition exploitation:* Crucially, we use that  $u_0^k$  satisfies the variational condition  $(\mathbf{P}_{\Omega, k})$ .

The interplay between (i) the analytic moment estimates and (ii) the variational structure of the optimization problem yields the desired error bounds.

**2.3. Proof of Theorem 2.2.** By the definition of the Kantorovich norm, there exists  $v^*$ , with  $\|v^*\|_{\mathcal{C}(\Omega)} \leq 1$  and  $\text{Lip}(v^*) \leq 1$ , such that

$$(2.13) \quad \|u_0^k - u_0^*\|_{\text{Kant}} = \int_{\Omega} v^* d(u_0^k - u_0^*).$$

We now estimate the right hand side expression in several steps.

**Step 1** (Decomposition of the r.h.s. of (2.13)). By Corollary 5.4, there exists a polynomial  $p_k$  of degree  $k$  such that

$$(2.14) \quad \|v^* - p_k\|_{\mathcal{C}(\Omega)} \leq \frac{C_d R}{2k},$$

where  $C_d$  is a constant depending only on the dimension  $d$ .

Let us write

$$(2.15) \quad \int_{\Omega} v^* d(u_0^k - u_0^*) = \underbrace{\int_{\Omega} (v^* - p_k) d(u_0^k - u_0^*)}_{\gamma_1} + \underbrace{\int_{\Omega} p_k d(u_0^k - u_0^*)}_{\gamma_2}.$$

In the following two steps, we estimate upper bounds of  $\gamma_1$  and  $\gamma_2$ , respectively.

**Step 2** (Estimate on  $\gamma_1$ ). Recalling the definition of the observation error  $\epsilon$ , by Lemma 2.7, there exists  $\tilde{u}_0 \in \mathcal{M}(\Omega)$ , such that

$$(2.16) \quad \int_{\Omega} x^\alpha d\tilde{u}_0(x) = (e^{-TA} \epsilon)_\alpha, \quad \text{for } \|\alpha\|_1 \leq k;$$

$$(2.17) \quad \|\tilde{u}_0\|_{\text{TV}} \leq \|\epsilon\|_\infty \underbrace{\sqrt{\frac{k}{\pi}} \exp\left(k\left(1 + 2d/R + \ln \sqrt{k}\right)\right)}_{=: \tilde{C}_{d,r}(k)} \max\left\{T^{\lfloor k/2 \rfloor}, 1\right\}.$$

Since  $u_0^*$  is the true initial distribution, we deduce from (2.16) that

$$\int_{\Omega} x^\alpha d(\tilde{u}_0 + u_0^*)(x) = (e^{-TA} \mathbf{y})_\alpha \quad \text{for } \|\alpha\|_1 \leq k.$$

Since  $u_0^k$  is a solution of  $(\mathbf{P}_{\Omega,k})$ , we have

$$\|u_0^k\|_{\text{TV}} \leq \|\tilde{u}_0 + u_0^*\|_{\text{TV}}.$$

By the triangle inequality,

$$\|u_0^k - u_0^*\|_{\text{TV}} \leq \|u_0^*\|_{\text{TV}} + \|u_0^k\|_{\text{TV}} \leq \|u_0^*\|_{\text{TV}} + \|\tilde{u}_0 + u_0^*\|_{\text{TV}} \leq 2\|u_0^*\|_{\text{TV}} + \|\tilde{u}_0\|_{\text{TV}}.$$

Combining with (2.14) and the a priori bound of  $\|\tilde{u}_0\|_{\text{TV}}$  in (2.17), it follows that

$$(2.18) \quad \gamma_1 \leq \frac{C_d R \|u_0^*\|_{\text{TV}}}{k} + \frac{C_d R}{2k} \tilde{C}_{d,R}(k) \max\left\{T^{\lfloor k/2 \rfloor}, 1\right\} \|\epsilon\|_\infty.$$

**Step 3** (Estimate on  $\gamma_2$ ). By (2.14), we have

$$\|p_k\|_{\mathcal{C}(\Omega)} \leq 1 + \frac{C_d R}{2k}.$$

Then, according to Lemma 5.5,

$$(2.19) \quad \sum_{\|\alpha\|_1 \leq k} |c_\alpha| \leq e^{\frac{2dk}{R}} \left(1 + \frac{C_d R}{2k}\right),$$

where  $c_\alpha$  are the coefficients of  $p_k$ . Letting  $u_0^k - u_0^*$  be the initial distribution of the heat equation, then the solution at time  $T$  has moments  $\epsilon_\alpha$  by the linearity of the heat equation. Therefore, we deduce from Lemmas 2.6 and 5.6 that

$$(2.20) \quad \left| \int_{\mathbb{R}^d} x^\alpha d(u_0^k - u_0^*) \right| \leq \sqrt{\frac{k}{\pi}} \exp\left(k + \frac{k}{2} \ln k\right) \max\{T^{\lfloor k/2 \rfloor}, 1\} \|\epsilon\|_\infty, \quad \text{for } \|\alpha\|_1 \leq k.$$

Recalling the definition of  $\gamma_2$  from (2.15), we have

$$(2.21) \quad \gamma_2 = \sum_{\|\alpha\|_1 \leq k} c_\alpha \int_{\mathbb{R}^d} x^\alpha d(u_0^k - u_0^*).$$

Recalling the definition of  $C_{d,r}(k)$  from (2.3) and combining (2.19)-(2.21), we obtain

$$(2.22) \quad \gamma_2 \leq \left(1 + \frac{C_d R}{2k}\right) \tilde{C}_{d,R}(k) \max\{T^{\lfloor k/2 \rfloor}, 1\} \|\epsilon\|_\infty.$$

The final estimate (2.2) follows from (2.13), (2.15), (2.18), and (2.22).

**2.4. Error estimate in Wasserstein distance.** The Kantorovich norm (see Definition 1.1) is introduced to quantify the distance between two signed measures that may have different total masses. In the case where the total mass is the same, the Wasserstein distance is a well-known metric for measuring the discrepancy between distributions. Indeed, in this case, we can also estimate the Wasserstein distance between the recovered distribution  $u_0^k$  and the true one  $u_0^*$ , see (2.25).

Let  $\Omega$  be a compact set. Let  $u_1$  and  $u_2$  be two signed measures in  $\mathcal{M}(\Omega)$  with the same total mass, i.e.,  $u_1(\Omega) = u_2(\Omega)$ . The Wasserstein-1 distance (also referred to as the Kantorovich-Rubinstein distance or the Earth Mover's Distance in the literature) is defined as

$$(2.23) \quad W_1(u_1, u_2) := \max_{\substack{v \in \mathcal{C}(\Omega) \\ \text{Lip}(v) \leq 1}} \int_{\Omega} v d(u_1 - u_2).$$

Compared to the Kantorovich distance defined in (1.11), the  $W_1$  distance removes the upper bound of 1 on the maximum norm of the test function  $v$ . As a result, the  $W_1$  distance is not applicable when  $u_1(\Omega) \neq u_2(\Omega)$ . Indeed, adding a constant  $c$  to  $v$  does not change its Lipschitz constant, but introduces an additional nonzero term  $\int_{\Omega} c d(u_1 - u_2)$  in the integral. By choosing  $c$  with arbitrarily large magnitude, one can make the right-hand side of (2.23) diverge to infinity.

Restricting  $u_1$  and  $u_2$  to the space of probability measures recovers the classical definition of the Wasserstein-1 distance in [33, Sec. 6].

In the case of equal total mass, the Wasserstein-1 distance is equivalent to the Kantorovich norm, as shown in [19, Eq. (1.20)]: If  $u_1(\Omega) = u_2(\Omega)$ , then

$$(2.24) \quad \|u_1 - u_2\|_{\text{Kant}} \leq W_1(u_1, u_2) \leq \max\{1, D_\Omega/2\} \|u_1 - u_2\|_{\text{Kant}},$$

where  $D_\Omega$  denotes the diameter of  $\Omega$ .

Therefore, in the context of Theorem 2.2, if we suppose that there is no error in the total mass observation, i.e.,  $\epsilon_0 = 0$ , then,

$$(2.25) \quad W_1(u_0^k, u_0^*) \leq \max\{1, \sqrt{d}R\} \|u_0^k - u_0^*\|_{\text{Kant}},$$

and  $\|u_0^k - u_0^*\|_{\text{Kant}}$  is bounded by (2.2).

We note that if the total mass of the initial distribution is known a priori (for example, if  $u_0^*$  is known to be a probability measure), then it can be preserved throughout the entire numerical resolution process. First, since the heat equation conserves total mass, we can directly set  $y_0$  to the known value, without needing to estimate it via quadrature methods. Next, the semigroup  $e^{-tA}$ , associated with the reverse moment dynamics, is a polynomial operator. As a result, computing  $e^{-tA}y$  introduces no numerical error, as it simply involves evaluating a polynomial in  $tA$  applied to

$y$ ; see Section 3.2 for the explicit formula. Finally, the moment constraints in the primal problem are given as equalities, ensuring that the total mass is exactly preserved in the final solution.

### 3. OBSERVATION, DISCRETIZATION, AND ALGORITHMS

This section is devoted to the numerical implementation of our moment-based method. Section 3.1 introduces two quadrature techniques for observing the moments of  $u(\cdot, T)$ , while Section 3.2 describes the discretization procedure and the optimization algorithm used to solve  $(P_{\Omega, k})$ .

#### 3.1. Observation of moments.

$$M_\alpha(T) = \int_{\mathbb{R}^d} x^\alpha u(x, T) dx.$$

is based on the observations of  $u(x, T)$  at specific sensor locations. Therefore, quadrature methods are used to approximate the integral. In the following paragraphs, two quadrature methods are presented.

**3.1.1. Uniform Quadrature.** The first and most direct way to compute  $M^\alpha(T)$  is via uniform quadrature, that is, by approximating the integral with a Riemann sum on a uniform grid. Specifically, we choose a large  $L > 0$  to bound the domain and discretize  $[-L, L]^d$  uniformly using  $n^d$  points (with  $n$  points along each edge). The grid points are denoted by  $x_\beta$  for  $\beta \in \mathbb{Z}_+^{*d}$  with  $\|\beta\|_\infty \leq n$ . The resulting approximation is given by:

$$(3.1) \quad M_\alpha(T) \approx \left(\frac{2L}{n}\right)^d \sum_{\|\beta\|_\infty \leq n} x_\beta^\alpha u(x_\beta, T).$$

In this method, the sensors are fixed at points  $x_\beta$  and hence their positions are independent of  $T$ . However, when  $T$  is large, the solution  $u(\cdot, T)$  becomes widely spread, meaning that the concentration within the hypercube  $[-L, L]^d$  decreases.

For example, if the initial distribution is  $\delta_0$ , then by the Gaussian tail estimate,  $(1 - \epsilon)$  of the mass of  $u(\cdot, T)$  is concentrated in the box  $[-L_{\epsilon, T}, L_{\epsilon, T}]^d$ , where  $L_{\epsilon, T}$  is of order  $\sqrt{T \ln(d/\epsilon)}$ . As a result, the discretization parameter  $n$  must be sufficiently large to accurately capture the solution. In conclusion, the uniform approach is straightforward to implement and works for small terminal times  $T$ , but for larger  $T$ , we instead propose the Gauss–Hermite method described below.

**3.1.2. Gauss–Hermite quadrature.** To derive the quadrature formula of this method, we first apply a change of variable to the moment integral by scaling  $x$  by a factor  $\sigma$  (to be determined later):

$$(3.2) \quad \int_{\mathbb{R}^d} x^\alpha u(x, T) dx = \sigma^{\|\alpha\|_1 + d} \int_{\mathbb{R}^d} z^\alpha u(\sigma z, T) dz.$$

Next, we rewrite the integral on the right-hand side of (3.2) as

$$(3.3) \quad \int_{\mathbb{R}^d} z^\alpha u(\sigma z, T) dz = \int_{\mathbb{R}^d} \underbrace{\left( z^\alpha u(\sigma z, T) e^{-\|z\|^2} \right)}_{=: g_\sigma(z)} e^{-\|z\|^2} dz.$$

By applying the Gauss–Hermite quadrature in dimension  $d$ , we obtain that

$$(3.4) \quad \int_{\mathbb{R}^d} g_\sigma(z) e^{-\|z\|^2} dz \approx \sum_{i_1=1}^n \cdots \sum_{i_d=1}^n \left( \prod_{j=1}^d \omega_{i_j} \right) g_\sigma(z_{i_1}, \dots, z_{i_d}),$$

where  $n \geq 1$  is the degree of quadrature,  $(\omega_i)_{i=1}^n$  and  $(z_i)_{i=1}^n$  denote the weights and nodes corresponding to the  $n$ -th Hermite polynomial (see [25, Sec. 18.3]).

For the quadrature to succeed, it is essential that  $g_\sigma(z_{i_1}, \dots, z_{i_d})$  remains within moderate bounds. Otherwise, numerical overflow may occur, especially since  $g_\sigma$  contains the exponential

factor  $e^{\|z\|^2}$ . However, the rapid spatial decay of the heat solution  $u(\cdot, T)$  compensates for this exponential growth if a reasonable scaling factor  $\sigma$  is chosen. Indeed, note that  $u(\sigma z, T)$  behaves like  $e^{-\|\sigma z\|^2/(4T)}$  (according to the formula for the heat kernel  $G$ ). Hence, we choose

$$(3.5) \quad \sigma = 2\sqrt{T}.$$

Therefore, by (3.2)–(3.5) we obtain the following complete approximation for  $M_\alpha(T)$ :

$$(3.6) \quad M_\alpha(T) \approx (2\sqrt{T})^{\|\alpha\|_1+d} \sum_{i_1=1}^n \cdots \sum_{i_d=1}^n \left( \prod_{j=1}^d \omega_{i_j} z_{i_j}^{\alpha_j} \right) \exp \left( \sum_{j=1}^d z_{i_j}^2 \right) u(2\sqrt{T}(z_{i_1}, \dots, z_{i_d}), T).$$

Compared to (3.1), the Gauss–Hermite quadrature features sensor positions that depend on  $T$ . Indeed, the positions

$$2\sqrt{T}(z_{i_1}, \dots, z_{i_d})$$

grow at a rate proportional to  $\sqrt{T}$ . Despite the inconvenience associated with moving sensors, our numerical simulations indicate that the Gauss–Hermite quadrature (3.6) yields superior results to the uniform quadrature (3.1) with the same number of sensors, see Figure 2 for a comparison.

**3.2. Discretize-then-optimize.** Since  $(P_{\Omega, k})$  is an optimization problem defined on an infinite-dimensional space, we adopt a discretize-then-optimize approach to solve it.

**3.2.1. Discretization.** We first discretize the domain  $\Omega$  by selecting a set of  $N$  points,

$$\Omega \xrightarrow{\text{discretize}} \Omega_h = \{x_1, \dots, x_N\}.$$

In this discrete setting, any initial condition  $u_0 \in \mathcal{M}(\Omega_h)$  can be expressed as a finite sum of Dirac measures:

$$u_0 = \sum_{i=1}^N m_i \delta_{x_i}.$$

Thus, the discretized version of  $(P_{\Omega, k})$  reduces to a finite-dimensional optimization problem in  $\mathbb{R}^N$ , with the optimization variables given by the vector of weights  $\mathbf{m} = (m_i)_{i=1}^N$ :

$$(P_{\Omega, k}^{\text{dis}}) \quad \inf_{\mathbf{m} \in \mathbb{R}^N} \|\mathbf{m}\|_{\ell^1} \quad \text{subject to} \quad B \mathbf{m} = e^{-TA} \mathbf{y},$$

where  $\mathbf{y} = (y_\alpha)_{\|\alpha\|_1 \leq k}$  denotes the observations of moments at time  $T$ , and

- $A$  is defined in (1.5). By Lemma 2.6,  $A$  is  $(\lfloor k/2 \rfloor + 1)$ -nilpotent, so that

$$e^{-TA} = \sum_{j=0}^{\lfloor k/2 \rfloor} \frac{(-A)^j}{j!} T^j;$$

- $B$  is a  $\binom{k+d}{d} \times N$  matrix with entries

$$b_{\alpha, i} = x_i^\alpha, \quad \text{for } \|\alpha\|_1 \leq k, \quad i = 1, \dots, N.$$

The non-emptiness of the admissible set for the discretized problem  $(P_{\Omega, k}^{\text{dis}})$  is nontrivial. This is because the monomials  $\{x^\alpha\}_{\|\alpha\|_1 \leq k}$  are not, in general, linearly independent in  $\mathcal{C}(\Omega_h)$ . To guarantee the feasibility of  $(P_{\Omega, k}^{\text{dis}})$ , we introduce the notion of a *unisolvant set*. A set of points  $\{z_i \in \mathbb{R}^d\}_{i=1, \dots, \binom{k+d}{d}}$  is said to be a unisolvant set of degree  $k$  if and only if the only polynomial  $p$  of degree at most  $k$  that satisfies

$$p(z_i) = 0 \quad \text{for all } i \leq \binom{k+d}{d}$$

is the zero polynomial, i.e.,  $p \equiv 0$ . Here, we give two examples of unisolvant sets:

- (1) If  $d = 1$ , then  $\{z_i \in \mathbb{R}\}_{i=1,\dots,k+1}$  is a unisolvant set of degree  $k$  if and only if  $z_i \neq z_j$  for any  $i \neq j$ .
- (2) If  $d = 2$ , then the family of Padua points [7, 6] up to degree  $k$  forms a unisolvant set of degree  $k$ . Suppose  $k$  is even, then the family of Padua points up to degree  $k$  is the collection of  $z_{i,j} = (z_i^1, z_j^2) \in \mathbb{R}^2$  for  $0 \leq i \leq k$  and  $0 \leq j \leq k/2$  with

$$z_i^1 = \cos\left(\frac{i\pi}{k}\right), \quad z_j^2 = \begin{cases} \cos\left(\frac{2j\pi}{k+1}\right), & \text{if } i \text{ is odd,} \\ \cos\left(\frac{(2j+1)\pi}{k+1}\right), & \text{if } i \text{ is even.} \end{cases}$$

**Lemma 3.1.** Suppose that  $N \geq \binom{k+d}{d}$  and that  $\Omega_h$  contains  $\binom{k+d}{d}$  points forming a unisolvant set of degree  $k$ . Then problem  $(P_{\Omega,k}^{\text{dis}})$  admits solutions for any  $\mathbf{y} \in \mathbb{R}^{\binom{k+d}{d}}$ .

*Proof.* The matrix  $B$  is a high-dimensional (rectangular) Vandermonde matrix. It has full row rank if it contains a square, invertible Vandermonde submatrix. According to [26, Thm. 4.1], this condition is equivalent to the existence of  $\binom{k+d}{d}$  points in  $\Omega_h$  that form a unisolvant set of degree  $k$ . In this case, the admissible set is non-empty and convex. The existence of a solution then follows from standard arguments based on the convexity and coercivity of problem  $(P_{\Omega,k}^{\text{dis}})$ .  $\square$

**3.2.2. Optimization.** Following the general idea in [10], we transform  $(P_{\Omega,k}^{\text{dis}})$  into an equivalent linear programming and employ the simplex method to solve it. The equivalent linear programming for  $(P_{\Omega,k}^{\text{dis}})$  is given by

$$(3.7) \quad \inf_{\mathbf{m}_+ \in \mathbb{R}_+^N, \mathbf{m}_- \in \mathbb{R}_+^N} \langle \mathbf{1}, \mathbf{m}_+ + \mathbf{m}_- \rangle \quad \text{subject to} \quad B(\mathbf{m}_+ - \mathbf{m}_-) = e^{-TA} \mathbf{y},$$

where  $\mathbf{1}$  is the  $N$ -dimensional vector of all ones.

**Proposition 3.2.** Under the setting of Lemma 3.1, problem (3.7) has solutions. Let  $(\mathbf{m}_+, \mathbf{m}_-)$  be the solution of (3.7) obtained from the simplex method. Then  $\mathbf{m} = \mathbf{m}_+ - \mathbf{m}_-$  is a solution of  $(P_{\Omega,k}^{\text{dis}})$  and  $\|\mathbf{m}\|_{\ell^0} \leq \binom{k+d}{d}$ .

*Proof.* The proof is the same as the proof of Theorem 4.7 in [22].  $\square$

#### 4. NUMERICAL SIMULATIONS

**4.1. Settings.** In our numerical experiments, we consider the heat equation (1.1) in dimensions  $d = 1$  and  $d = 2$ , with initial data given by six Dirac masses whose locations and amplitudes are chosen at random. The exact positions and amplitudes are listed in Table 1 and depicted in the first row of Figure 1.

	1	2	3	4	5	6
Position (1D)	-3.11	2.16	-2.13	0.3	-4.37	3.77
Amplitude (1D)	4.0071	-4.6658	4.5695	-3.6279	-2.1617	1.0608
Position (2D)	(-1.30, -2.27)	(-1.43, 0.08)	(3.9, -3.69)	(3.72, 2.57)	(3.04, -0.91)	(-3.96, -0.52)
Amplitude (2D)	2.6832	0.6610	-2.5463	0.4501	-3.5543	-0.5107

TABLE 1. Support Positions and Amplitudes of  $u_0^*$

The moments are computed using quadrature methods based on the values of  $u(x_i, T)$ , where  $x_i$  denotes the positions of the sensors used in the corresponding quadrature rule. The values  $u(x_i, T)$  are computed using the closed-form solution of the heat equation. Since the initial distribution is

a sum of Dirac delta functions, the solution is expressed as a sum of Gaussian distributions. This approach avoids numerical errors associated with discretizing the heat equation. Aside from this, the initial distribution is not incorporated into the optimization process. The second row of Figure 1 shows solutions at one terminal time  $T = 10$  over their proper domain, clearly demonstrating that recovering the initial distribution  $u_0$  is highly non-trivial.

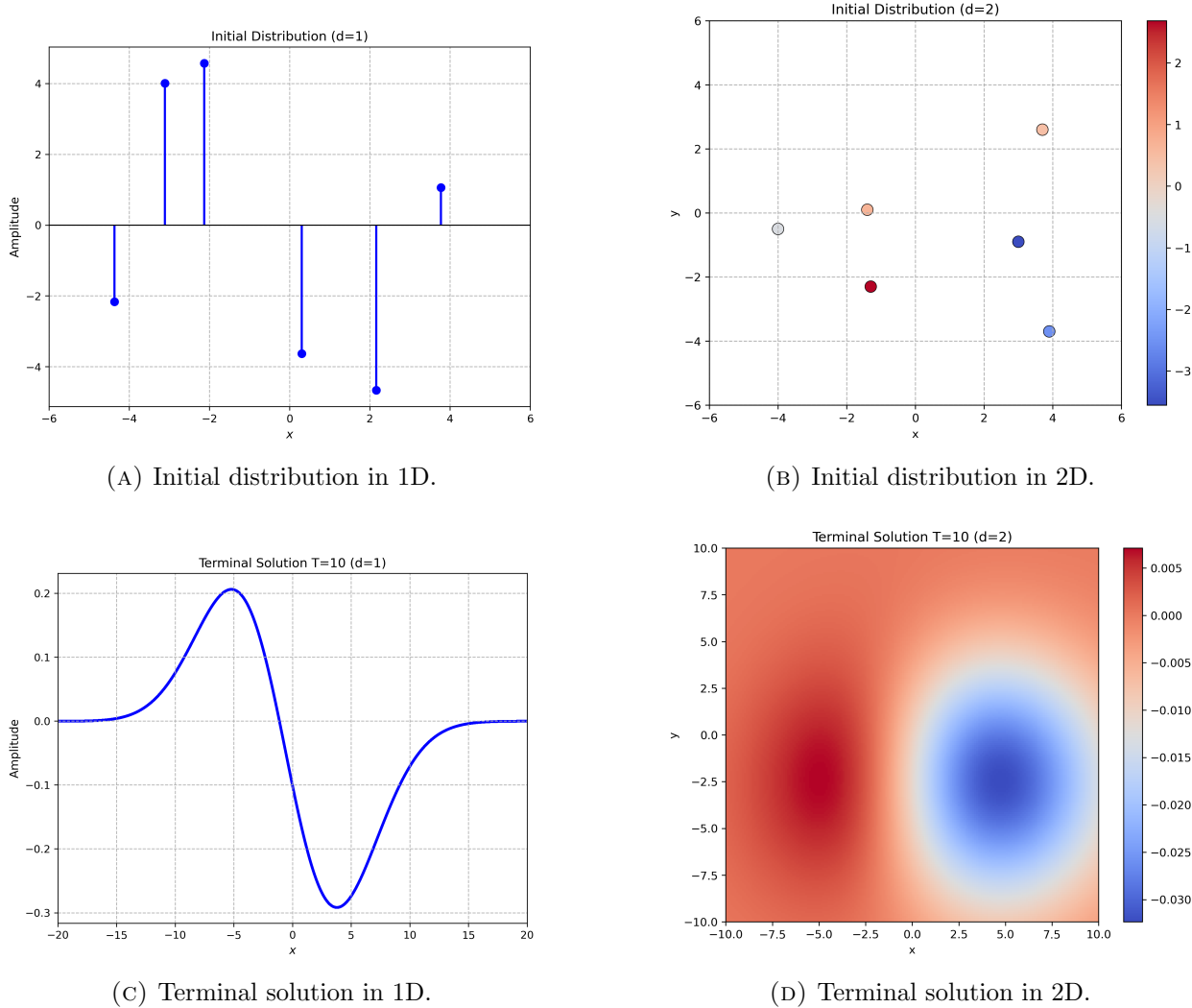


FIGURE 1. Initial conditions and terminal solutions ( $T = 10$ ) of (1.1).

4.1.1. *Quadrature of moments.* We present here the settings and observations of quadrature methods to obtain the moments in the one-dimensional case; the behavior in two dimensions is qualitatively similar.

For the uniform quadrature method, we integrate over the domain  $[-50, 50]$  and vary the number of discretization points  $n$  from 2 to 100. For the Gauss–Hermite quadrature, we use up to the first 100 weights and nodes associated with the Hermite polynomials. Figure 2(A) compares the error of these two methods for the fourth-order moment of  $u(\cdot, T)$ , with  $T = 10$  fixed. The results clearly show that Gauss–Hermite quadrature achieves greater accuracy than the uniform method for the same number of sensors. However, when the number of sensors is sufficiently large, both quadrature schemes yield reliable moment estimates at  $T = 10$ . This implies that for moderately sized terminal

times, a sufficiently dense uniform grid can replace Gauss–Hermite quadrature without the need to move sensor locations according to the Gaussian weights in (3.6).

For larger values of  $T$ , as shown in Figure 2(B), the errors from both quadrature methods increase, but Gauss–Hermite quadrature remains significantly more stable than the uniform approach. In fact, for large  $T$ , the uniform method requires both a larger integration domain and a substantially greater number of sensors to achieve comparable accuracy.

In Figure 2(C), we compare the moment errors at time 0 obtained via Gauss–Hermite quadrature combined with the inversion of the moment equation (1.5). The error is defined by

$$(4.1) \quad \|M(0) - e^{-TA} \mathbf{y}\|_\infty,$$

where  $A$  is the generator of the semigroup in (1.5), and  $\mathbf{y} = (y_0, \dots, y_k)$  is computed using Gauss–Hermite quadrature with 100 sensors. We observe that the error increases rapidly with the moment order  $k$ . For small terminal times (e.g.,  $T = 1$  and  $T = 10$ ), the moments remain accurate up to  $k = 14$ , enabling good recovery of the initial distribution, as illustrated later in Figure 3. However, for large terminal times (e.g.,  $T = 1000$ ), the moment error becomes substantial for high  $k$ , which explains why the moment method is reliable only for low-order moments in such cases. Despite this, the numerical results for  $(T, k) = (1000, 10)$  still provide a reasonable approximation of the initial distribution, as shown in Figure 3.

**4.1.2. Discretization and optimization parameters.** Based on our previous quadrature results, we use the values  $y_k$  obtained via Gauss–Hermite quadrature with  $10^2$  and  $10^4$  sensors in one and two dimensions, respectively. The a priori domain  $\Omega$  for the initial distribution is taken to be  $[-5, 5]$  in one dimension and  $[-5, 5]^2$  in two dimensions.

We then discretize  $\Omega$  using a uniform mesh, yielding the discrete domain  $\Omega_h$  and the fully discretized problem  $(P_{\Omega, k}^{\text{dis}})$ . In the one-dimensional case, this mesh is a unisolvant set of degrees of discretization. In two dimensions, the uniform mesh achieves results comparable to those obtained with the Padua points, so we opt for the simpler uniform grid. The matrix  $B$  in the discretized problem  $(P_{\Omega, k}^{\text{dis}})$  has dimensions  $N \times \binom{k+d}{d}$ . This matrix must be stored in the computer’s RAM when applying the simplex method. To accommodate this constraint, we set  $N = 10^3$  for the one-dimensional case and  $N = 10^4$  for the two-dimensional case. These choices limit the maximum allowable moment order  $k$ , as larger values can lead to memory overflow. All numerical simulations are performed on a laptop equipped with 16 GB of RAM. To avoid any loss of numerical precision in the matrix  $B$ , we fix the maximum moment order to  $k_{\max} = 16$  in one dimension and  $k_{\max} = 10$  in two dimensions. For the 1D case, we test with terminal times  $T = 1, 10, 100, 1000$ , and for the 2D case,  $T$  is set to 100. The table below summarizes all the parameters used in our experiments.

Parameter	1D Case	2D Case
Quadrature method	Gauss–Hermite	Gauss–Hermite
Number of sensors $n$	$10^2$	$10^4$
A priori domain $\Omega$	$[-5, 5]$	$[-5, 5]^2$
Discretization method	Uniform mesh (unisolvant)	Uniform mesh
Discretization size $N$	$10^3$	$10^4$
Max moment order $k_{\max}$	16	10
Terminal times $T$	1, 10, 100, 1000	100
Hardware	Intel(R) Core(TM) i5-1335U, 16 GB RAM	

TABLE 2. Summary of parameters used in the numerical experiments.

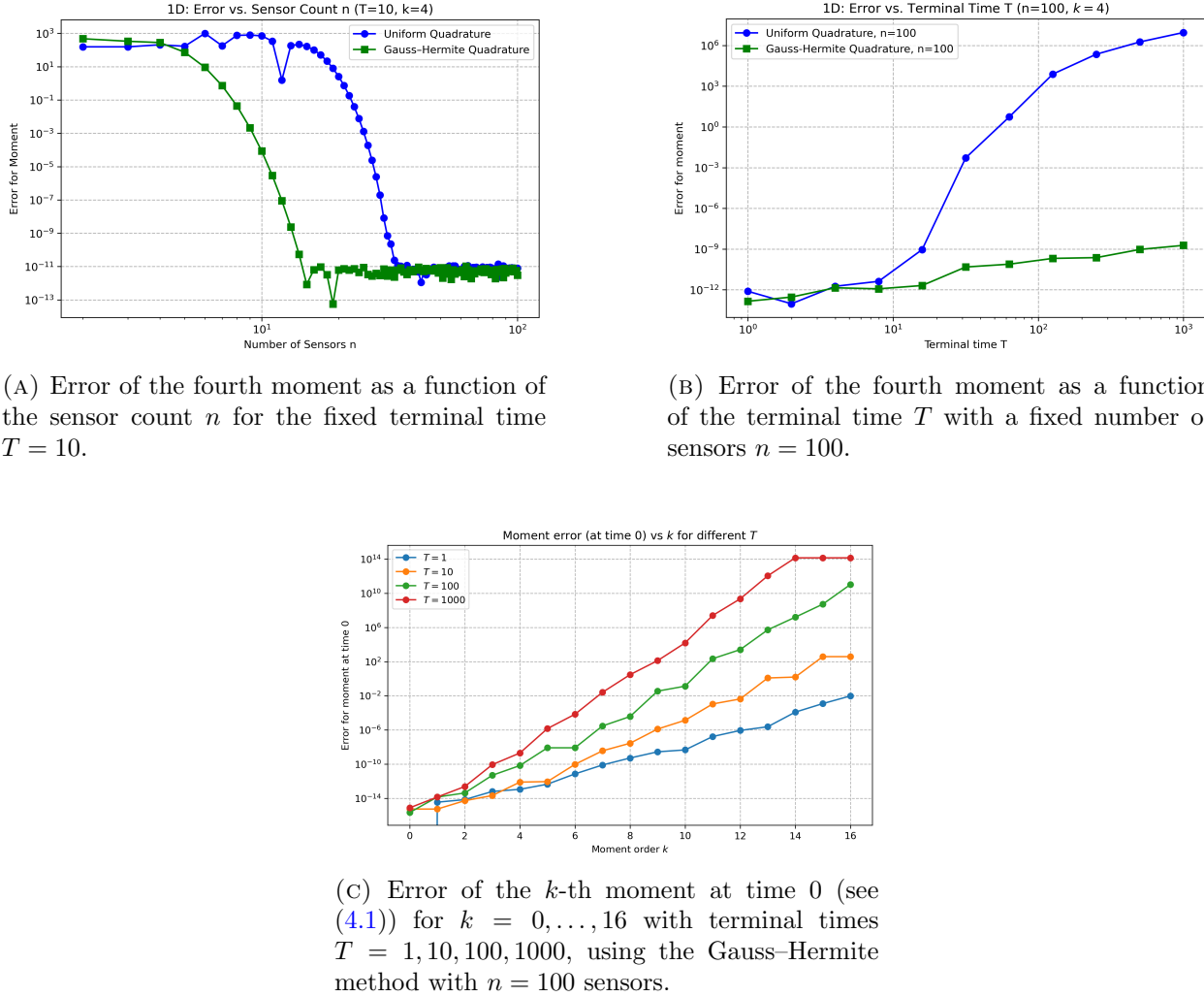


FIGURE 2. Moment errors obtained with the quadrature methods. (a) Varying sensor count  $n \in \{1, \dots, 100\}$  at fixed  $T = 10$ . (b) Varying terminal time  $T \in [1, 1000]$  at fixed  $n = 100$ . (c) Joint influence of moment order  $k$  and terminal time for the Gauss–Hermite scheme.

**4.2. Numerical results.** The numerical results for the one- and two-dimensional experiments are presented in Figures 3 and 4, respectively. In our numerical examples, the quadrature used to compute the total mass ( $\alpha = 0$ ) remains highly accurate, with errors on the order of  $10^{-15}$  even for  $T = 1000$ . Therefore, following the discussion in Section 2.4, we use the Wasserstein-1 ( $W_1$ ) distance to evaluate the discrepancy between the recovered initial distribution  $u_0^k$  and the true distribution  $u_0^*$ . This distance can be computed using the optimal transport formulation of  $W_1$ . In particular, since both measures are finite sums of Dirac masses, the optimal transport problem reduces to a linear programming problem, which can be solved by the simplex method.

**4.2.1. The one-dimensional case.** In Figure 3(A), we show the evolution of  $W_1(u_0^k, u_0^*)$  for  $k \leq 16$  across different terminal times  $T = 1, 10, 100$ , and  $1000$ . In Figure 3(B), we take the best moment number  $k$  for each  $T$  and plot the recovered initial distributions. Several observations can be made:

- (1) When  $k$  is small, the four curves corresponding to different terminal times coincide and exhibit similar decreasing behavior. This is because the quadrature errors for these moments

are very small (refer to Figure 2(C)), and the second term in our error estimate (2.2) is polynomial with respect to  $T$ . Thus, the second term is negligible compared to the first term, which decreases at the rate  $\mathcal{O}(1/k)$  and is independent of  $T$ .

- (2) As  $k$  increases, the exponential instability associated with large  $k$  becomes apparent, particularly for large values of  $T$ . Specifically, for  $T = 1000$ , the error curve starts to diverge notably after  $k = 10$ ; similar phenomena are observed for  $(T, k) = (100, 12)$  and  $(10, 14)$ . For  $T = 1$ , the error reduces to approximately  $10^{-6}$  after 14 moments, demonstrating the strong performance of our moment method, especially when compared to results in [21, 4], where  $T = 0.01$  is used.
- (3) A sharp decrease is observed for  $T = 1$  and  $T = 10$  between moment orders  $k = 13$  and  $k = 14$ . This is an interesting phenomenon that goes beyond the theoretical decay rate of  $1/k$  (which is indeed observed up to  $k = 13$ ). This behavior is illustrated in the second and third subplots of Figure 3(B): at  $k = 13$ , the recovery is similar to that at  $k = 12$ , while at  $k = 14$ , all true Dirac positions are successfully recovered. The subsequent improvements mainly concern the amplitudes, as shown in the first subplot, where some negligible amplitudes are removed comparing to  $k = 14$ . A full theoretical explanation of this phenomenon is beyond the scope of the current work and is proposed as a direction for future research.
- (4) For  $T = 100$  and  $T = 1000$ , the best Wasserstein distances remain at the order of  $10^1$ . However, the recovered distributions provide good approximations of the true support points of  $u_0^*$ . This suggests that a sparse grid strategy could be employed as a post-processing step: namely, by refining the mesh  $\Omega_h$  around the recovered support points and subsequently optimizing the amplitudes at these refined nodes.

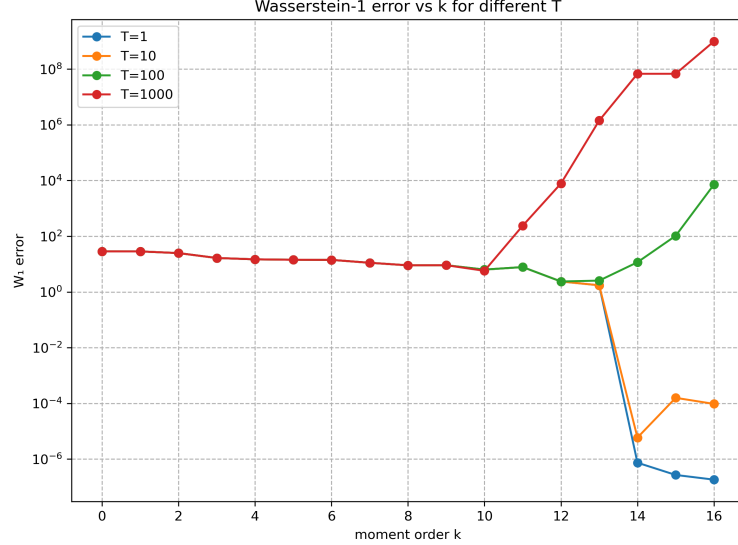
**4.2.2. The two-dimensional case.** In the two-dimensional case, we fix the maximum moment order to  $k_{\max} = 10$  and the terminal time to  $T = 100$ . Consequently, the discretized solution may exhibit up to  $\binom{12}{2} = 66$  support points—far more than the true distribution. Nevertheless, these points cluster tightly around a few centers, which serve as excellent approximations to the true Dirac support locations of  $u_0^*$ . To reduce this redundancy, we merge any points whose pairwise distance is below a threshold 0.02. Each resulting cluster is then replaced by its amplitude-weighted barycenter, with the cluster amplitude equal to the sum of its constituent amplitudes. This simple post-processing step substantially improves the accuracy of the recovered measure.

Figure 4 illustrates the performance of the recovered distribution  $u_0^k$  obtained by solving  $(P_{\Omega, k}^{\text{dis}})$  and the post-processing step. We have the following observations:

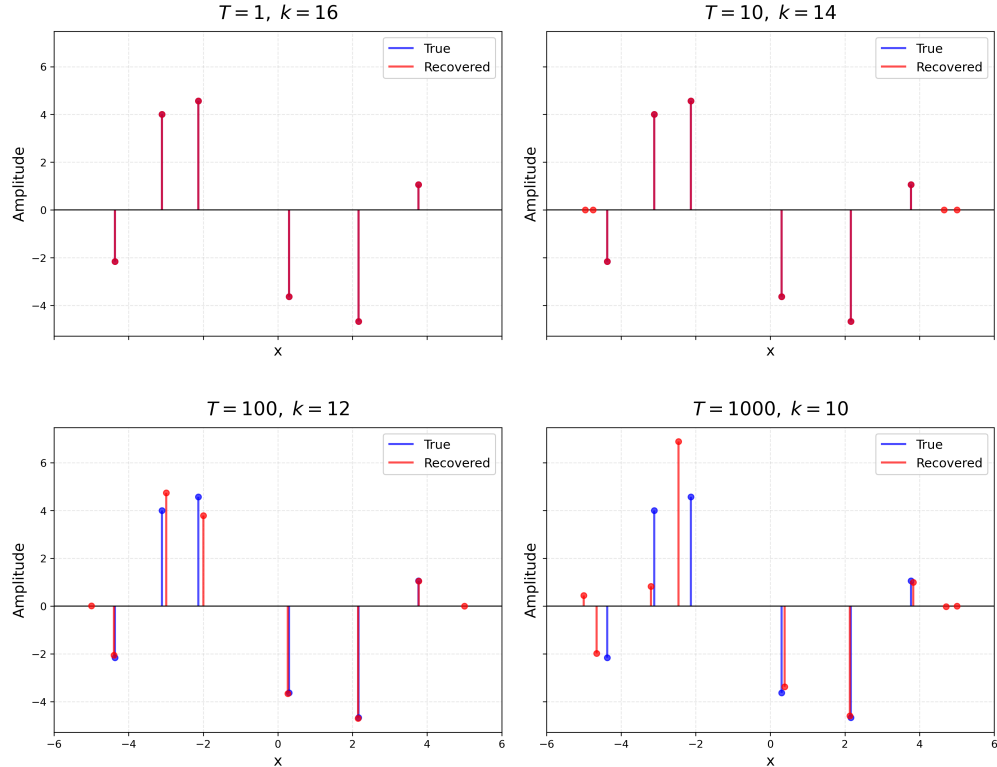
- (1) In Figure 4(A), the  $W_1$  error displays a trend analogous to the one-dimensional case: it decreases initially, exhibits a sharp drop between  $k = 6$  and  $k = 8$ , and then begins to increase again from  $k = 9$ . Figure 4(B) reveals that at  $k = 6$ , the recovered support points are broadly scattered, although the most significant locations (dark markers) are already detected. At  $k = 7$ , these points begin to cluster around the key positions, and by  $k = 8$ , the groups have merged very close to the true support points of  $u_0^*$ .
- (2) Even for  $T = 100$ , the recovered distributions remain highly accurate, demonstrating that the moment method's performance is not sensitive to the dimension  $d$ . This follows from our error bound (2.2), in which the polynomial degree on  $T$  involves only the moment order  $k$  and not the dimension  $d$ . Consequently, the maximum feasible terminal time retains a similar order of magnitude as in lower-dimensional settings.

## 5. TECHNICAL LEMMAS AND PROOFS

**5.1. A Representer Theorem.** We first recall a representer theorem from [16, Thm. 1], which plays the essential role in the proof of Theorem 2.1.



(A) Evolution of  $W_1(u_0^k, u_0^*)$  by  $k$  for terminal times  $T = 1, 10, 100, 1000$ .



(B) Comparison of  $u_0^k$  (with  $k$  chosen to minimize  $W_1$ ) and  $u_0^*$  for  $T = 1, 10, 100, 1000$ .

FIGURE 3. Numerical results for the 1D case: (A) Values of  $W_1(u_0^k, u_0^*)$  for  $k \in [0, 16]$  and  $T = 1, 10, 100, 1000$ . (B) Recovered initial distributions  $u_0^k$  versus the true  $u_0^*$ , where  $k$  minimizes the  $W_1$  distance from (A).

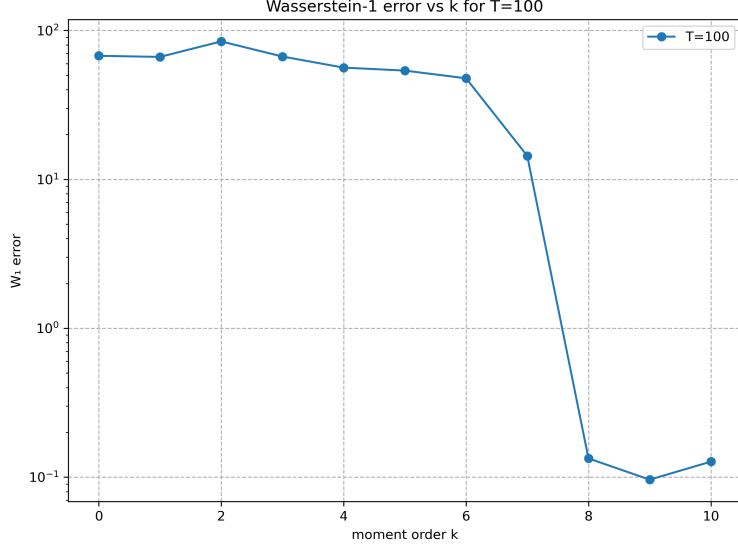
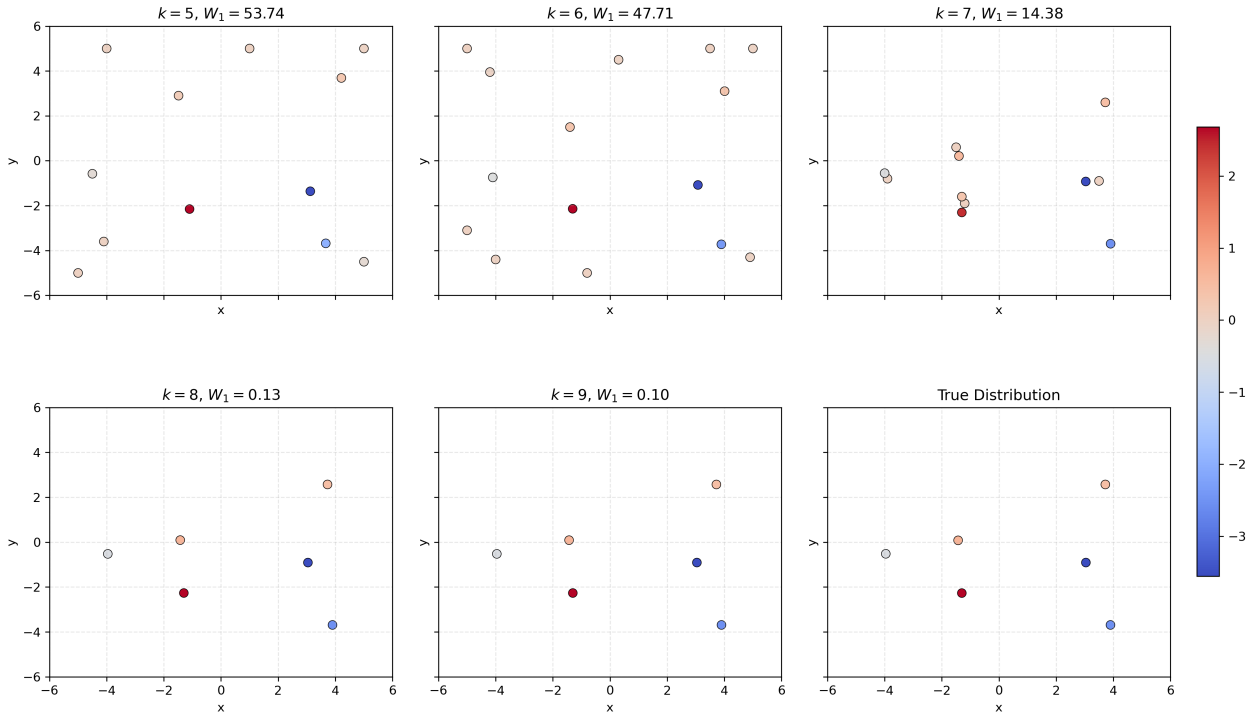
(A) Evolution of  $W_1(u_0^k, u_0^*)$  by  $k$  for terminal time  $T = 100$ .(B) Solutions of  $(P_{\Omega,k})$  (after clustering) with  $k = 5, \dots, 9$ ,  $T = 100$ , and the true distribution.

FIGURE 4. Numerical results for the 2D case: (A) Values of  $W_1(u_0^k, u_0^*)$  for  $k \in [0, 10]$  and  $T = 100$ . (B) Recovered initial distributions  $u_0^k$  for  $k = 5, \dots, 9$ , versus the true  $u_0^*$ .

**Theorem 5.1** (Fisher-Jerome 75). *Let  $\Omega$  be a compact set in  $\mathbb{R}^d$ . Let  $N \in \mathbb{Z}_+$  and  $l_i: \Omega \rightarrow \mathbb{R}$  be continuous functions for  $i = 1, \dots, N$ . Consider the following optimization problem:*

$$(5.1) \quad \inf_{\mu \in \mathcal{M}(\Omega)} \|\mu\|_{\text{TV}}, \quad \text{s.t. } \int_{\Omega} l_i(\theta) d\mu(\theta) \in I_i, \quad \text{for } i = 1, \dots, N,$$

where  $I_i$  is a compact interval or a singleton in  $\mathbb{R}$  for  $i = 1, \dots, N$ . Assume that the feasible set of problem (5.1) is non-empty. Then, its solution set is non-empty, convex, and compact in the weak-\* sense. Moreover, the extreme points of the solution set of (5.1) are of the form:

$$\mu^* = \sum_{i=1}^N \omega_i \delta_{x_i},$$

where  $\omega_i \in \mathbb{R}$  and  $x_i \in \Omega$  for  $i = 1, \dots, N$ .

**Lemma 5.2.** *Fix any  $k \geq 0$ . Let  $\Omega$  be a compact subset of  $\mathbb{R}^d$  such that  $[-r, r]^d \subseteq \Omega$  for some  $r > 0$ . Consider the moment problem*

$$(5.2) \quad \inf_{\mu \in \mathcal{M}(\Omega)} \|\mu\|_{\text{TV}}, \quad \text{subject to } \int_{\Omega} x^{\alpha} d\mu(x) = z_{\alpha}, \quad \text{for all } \|\alpha\|_1 \leq k,$$

where  $\mathbf{z} = (z_{\alpha})_{\|\alpha\|_1 \leq k} \in \mathbb{R}^{\binom{k+d}{d}}$  is an arbitrary vector. Let  $\mu^*$  be any solution of problem (5.2). Then, the total variation of  $\mu^*$  satisfies the following a priori estimate:

$$(5.3) \quad \|\mu^*\|_{\text{TV}} \leq e^{\frac{2dk}{r}} \|\mathbf{z}\|_{\infty}.$$

*Proof.* Since  $\Omega$  contains a nonempty interior, the collection of monomials  $\{x^{\alpha}: \Omega \rightarrow \mathbb{R}\}_{\|\alpha\|_1 \leq k}$  is linearly independent. Hence, the existence of a solution  $\mu^*$  follows from Theorem 5.1.

The dual problem of (5.2) is given by (see [13, Sec. 2.3])

$$(5.4) \quad \sup_{c_{\alpha}} \sum_{\|\alpha\|_1 \leq k} z_{\alpha} c_{\alpha} \quad \text{subject to} \quad \sup_{x \in \Omega} \left| \sum_{\|\alpha\|_1 \leq k} c_{\alpha} x^{\alpha} \right| \leq 1.$$

By the Fenchel–Rockafellar theorem, strong duality holds (see [13, Prop. 13] for details):

$$\|\mu^*\|_{\text{TV}} = \text{val (5.2)} = \text{val (5.4)}.$$

Let  $\mathbf{c}^* = (c_{\alpha}^*)_{\|\alpha\|_1 \leq k}$  be a solution of (5.4). By Hölder's inequality, we have

$$\text{val (5.4)} \leq \|\mathbf{c}^*\|_1 \|\mathbf{z}\|_{\infty}.$$

Moreover,

$$\sup_{x \in \Omega} \left| \sum_{\|\alpha\|_1 \leq k} c_{\alpha}^* x^{\alpha} \right| \leq 1.$$

Since  $\Omega$  contains  $[-r, r]^d$ , it follows from Lemma 5.5 that

$$\|\mathbf{c}^*\|_1 \leq e^{\frac{2dk}{r}}.$$

Therefore, the conclusion follows.  $\square$

### 5.2. Results from approximation theory.

**Lemma 5.3** (Jackson's Theorem in  $\mathbb{R}^d$  [24]). *For any  $L$ -Lipschitz function  $v$  defined on  $[-1, 1]^d$  and any  $k \geq 0$ , there exists a multivariable polynomial  $p_k$  of degree less than  $k$  such that*

$$\|v - p_k\|_{\mathcal{C}([-1, 1]^d)} \leq \frac{C_d L}{2k},$$

where  $C_d$  is a constant depending only on the dimension  $d$ .

**Corollary 5.4.** *Let  $\Omega = [-R, R]^d$  for some  $R > 0$ . For any function  $v \in \mathcal{C}(\Omega)$  satisfying  $\text{Lip}(v) \leq 1$  and any  $k \geq 0$ , there exists a multivariable polynomial  $p_k$  of degree less than  $k$  such that:*

$$\|v - p_k\|_{\mathcal{C}(\Omega)} \leq \frac{C_d R}{2k},$$

where  $C_d$  is a constant depending only on the dimension  $d$ .

*Proof.* It suffices to apply Lemma 5.3 to the rescaled function  $\bar{v}: [-1, 1]^d \rightarrow \mathbb{R}$ ,  $x \mapsto v(Rx)$ .  $\square$

**Lemma 5.5.** *Let  $f$  be any multivariable polynomial of degree less than  $k$ . Assume that for  $r > 0$ ,  $|f(x)| \leq 1$  for all  $x \in [-r, r]^d$ . Then, the following holds:*

$$\sum_{\|\alpha\|_1 \leq k} |c_\alpha| \leq e^{\frac{2dk}{r}},$$

where  $c_\alpha$  are the coefficients of  $f$ .

*Proof.* Fix any multi-index  $\alpha = (\alpha_1, \dots, \alpha_d) \in \mathbb{Z}_+^d$  with  $\|\alpha\|_1 \leq k$ . Recall that the Taylor coefficient of  $f$  at 0 corresponding to  $\alpha$  is given by

$$c_\alpha = \frac{1}{\alpha!} \frac{\partial^\alpha f(0)}{\partial x^\alpha} = \frac{1}{\alpha!} \frac{\partial^{\alpha_1} \partial^{\alpha_2} \dots \partial^{\alpha_d} f(0)}{\partial x_1^{\alpha_1} \partial x_2^{\alpha_2} \dots \partial x_d^{\alpha_d}}.$$

**Step 1** (Reduction to a univariate polynomial). Fix any  $(x_1, \dots, x_{d-1}) \in [-r, r]^{d-1}$  and consider  $f$  as a univariate function in the variable  $x_d$ . Since

$$|f(x)| \leq 1 \quad \text{for all } x \in [-r, r]^d,$$

we apply Bernstein's inequality for higher derivatives (see, e.g., [5, Sec. 5.2.E.5]) to deduce that for any fixed  $(x_1, \dots, x_{d-1})$

$$\left| \frac{\partial^{\alpha_d} f}{\partial x_d^{\alpha_d}}(x_1, x_2, \dots, x_{d-1}, 0) \right| \leq \left( \frac{2\alpha_d}{r} \right)^{\alpha_d}.$$

**Step 2** (Induction on the number of variables). Now, fix  $x_d = 0$ , and define

$$g(x_1, \dots, x_{d-1}) = \frac{\partial^{\alpha_d} f}{\partial x_d^{\alpha_d}}(x_1, \dots, x_{d-1}, 0).$$

Then  $g$  is a polynomial in  $(x_1, \dots, x_{d-1})$  of total degree at most  $k - \alpha_d$  and

$$\|g\|_{\mathcal{C}([-r, r]^{d-1})} \leq \left( \frac{2\alpha_d}{r} \right)^{\alpha_d}.$$

Applying the same argument as in Step 1, we

$$\left| \frac{\partial^{\alpha_{d-1}} g}{\partial x_{d-1}^{\alpha_{d-1}}}(x_1, \dots, x_{d-2}, 0) \right| \leq \left( \frac{2k}{r} \right)^{\alpha_d} \left( \frac{2(k - \alpha_d)}{r} \right)^{\alpha_{d-1}}.$$

Proceeding inductively over the remaining variables yields:

$$|c_\alpha| \leq \frac{(2k)^{\alpha_d} (2(k - \alpha_d))^{\alpha_{d-1}} \dots (2(k - \sum_{j=2}^d \alpha_j))^{\alpha_1}}{r^{\|\alpha\|_1} \alpha_1! \alpha_2! \dots \alpha_d!}.$$

It follows that

$$|c_\alpha| \leq \frac{(2k)^{\alpha_1+\alpha_2+\dots+\alpha_d}}{r^{\|\alpha\|_1} \alpha!} = \frac{1}{\alpha!} \left( \frac{2k}{r} \right)^{\|\alpha\|_1}.$$

**Step 3** (Summing over all multi-indices). Summing these estimates over all  $\alpha$  with  $\|\alpha\|_1 \leq k$ , we have

$$\sum_{\|\alpha\|_1 \leq k} |c_\alpha| \leq \sum_{\|\alpha\|_1 \leq k} \frac{1}{\alpha!} \left( \frac{2k}{r} \right)^{\|\alpha\|_1} = \sum_{j=0}^k \sum_{\|\alpha\|_1=j} \frac{1}{\alpha!} \left( \frac{2k}{r} \right)^j.$$

A standard combinatorial identity shows that

$$\sum_{\|\alpha\|_1=j} \frac{1}{\alpha!} = \frac{d^j}{j!},$$

so that

$$\sum_{\|\alpha\|_1 \leq k} |c_\alpha| = \sum_{j=0}^k \frac{1}{j!} \left( \frac{2dk}{r} \right)^j \leq e^{\frac{2dk}{r}}.$$

Thus, the proof is complete.  $\square$

**Lemma 5.6.** *For any  $k \geq 1$  and  $T > 0$ , we have*

$$\sum_{j=0}^{\lfloor k/2 \rfloor} \frac{k^j(k-1)^j}{j!} T^j \leq \sqrt{\frac{k}{\pi}} \exp \left( k + \frac{k}{2} \ln k \right) \max \left\{ T^{\lfloor k/2 \rfloor}, 1 \right\}.$$

*Proof.* By Hölder's inequality, we have

$$\sum_{j=0}^{\lfloor k/2 \rfloor} \frac{k^j(k-1)^j}{j!} T^j \leq \max \left\{ T^{\lfloor k/2 \rfloor}, 1 \right\} \sum_{j=0}^{\lfloor k/2 \rfloor} \frac{k^j(k-1)^j}{j!}.$$

It remains to bound the sum

$$S := \sum_{j=0}^{\lfloor k/2 \rfloor} \frac{k^j(k-1)^j}{j!}.$$

Let us first consider the case where  $k$  is even. Let  $k = 2m$ . Then

$$S \leq 1 + m \cdot \frac{k^m(k-1)^m}{m!}.$$

Using Stirling's lower bound

$$n! \geq \sqrt{2\pi n} \left( \frac{n}{e} \right)^n, \quad \text{for } n \in \mathbb{Z}_+,$$

we obtain

$$\frac{k^m(k-1)^m}{m!} \leq \frac{k^m(k-1)^m}{\sqrt{2\pi m} \left( \frac{m}{e} \right)^m} = \frac{1}{\sqrt{2\pi m}} \left( \frac{e^2 k(k-1)}{m^2} \right)^m.$$

Since  $m = k/2$ , we have

$$\frac{k^m(k-1)^m}{m!} \leq \frac{1}{\sqrt{\pi k}} (2e(k-1))^{k/2} = \frac{1}{\sqrt{\pi k}} \exp \left( \frac{k}{2} \ln(2e(k-1)) \right).$$

Therefore,

$$S \leq 1 + \frac{1}{2} \sqrt{\frac{k}{\pi}} \exp \left( k + \frac{k}{2} \ln(k-1) \right), \quad \text{for even } k.$$

Then for the odd case  $k = 2m+1$ , a similar argument gives

$$S \leq 1 + m \cdot \frac{k^m(k-1)^m}{m!} \leq 1 + \frac{1}{2} \sqrt{\frac{k-1}{\pi}} \exp \left( k - 1 + \frac{k-1}{2} \ln k \right), \quad \text{for odd } k \geq 3.$$

In both cases, we can bound uniformly for all  $k \geq 2$  by

$$S \leq 1 + \frac{1}{2} \sqrt{\frac{k}{\pi}} \exp\left(k + \frac{k}{2} \ln k\right) \leq \sqrt{\frac{k}{\pi}} \exp\left(k + \frac{k}{2} \ln k\right).$$

One easily checks that the inequality also holds for  $k = 1$ . Therefore, the desired result follows.  $\square$

## 6. CONCLUSION AND PERSPECTIVES

In this article, we introduced a moment-based approach to the inverse source identification problem for the heat equation, a classically ill-posed problem. The key idea is to reformulate the original problem via a moment system, which mitigates the time-related ill-posedness of the backward heat equation. The proposed scheme proceeds in two main steps:

- (1) inversion of the moment system to recover the moments of the initial distribution from noisy measurements;
- (2) reconstruction of the initial source by minimizing the total variation under the recovered moment constraints.

We further established an error estimate for the reconstructed distribution in the Kantorovich distance, which depends on the moment order, terminal time, and observation noise.

From an algorithmic perspective, we detailed how moments at terminal time can be estimated using quadrature techniques, and discussed the discretization and numerical solution of the resulting constrained optimization problem. Numerical experiments demonstrate the effectiveness of our approach. In particular, our method achieves robust recovery of the initial data for terminal times up to  $T = 100$ , significantly improving over existing benchmarks in the literature, which are typically limited to very small times (e.g.,  $T \approx 0.01$ ).

*Perspectives.* Here are some directions for future work related to this article:

- (1) (Heat equation with boundary conditions). When the heat equation (1.1) is posed with boundary conditions (for example, the Dirichlet condition  $u(x, t) = 0$  on  $\partial\Omega$ ), the ODE system (1.5) no longer accurately captures the evolution of the moments. One alternative is to replace the raw moments by the modal coefficients

$$a_m(t) = \int_{\Omega} u(x, t) \varphi_m(x) \, dx,$$

where  $\{\varphi_m\}$  are the Dirichlet eigenfunctions on  $\Omega$ . These coefficients satisfy a closed (though non-nilpotent) ODE system, but its inversion is typically less stable in time than the boundary-free moment method we have developed. A more pragmatic approach is simply to apply our moment method while ignoring the boundary conditions. For short time horizons ( $T$  small), the influence of the boundaries is mild, and this “unadjusted” method can still yield accurate numerical results.

- (2) (Advection-Diffusion Dynamics). A natural extension of the heat equation is the advection-diffusion process:

$$\begin{cases} \partial_t m - \operatorname{div}(D \nabla m - v m) = 0, & \text{for } (x, t) \in \mathbb{R}^n \times \mathbb{R}_+, \\ m(0, x) = m_0(x), & \text{for } x \in \mathbb{R}^n, \end{cases}$$

where  $D$  is a positive-definite diffusion matrix and  $v$  is the advection (drift) vector. The density  $m(t, x)$  describes the law of the stochastic process

$$\begin{cases} dX_t = v \, dt + \sqrt{2} D^{1/2} \, dW_t, \\ X_0 \sim m_0, \end{cases}$$

with  $\{W_t\}_{t>0}$  a standard Brownian motion. The initial source identification problem seeks to recover the distribution  $m_0$  by some information of  $m(T)$ . Our moment method is especially effective when  $D$  and  $v$  are spatially invariant and piecewise constant in time. In this setting, the resulting system of moment ODEs is closed and nilpotent. For space-dependent  $D$  and  $v$ , the problem becomes significantly more complex and remains a subject for future investigation.

## REFERENCES

- [1] Francis Bach. Breaking the curse of dimensionality with convex neural networks. *Journal of Machine Learning Research*, pages 1–53, 2017.
- [2] Christian Bayer and Josef Teichmann. The proof of Tchakaloff’s theorem. *Proceedings of the American Mathematical Society*, 134(10):3035–3040, 2006.
- [3] Dimitris Bertsimas and John Tsitsiklis. *Introduction to linear optimization*. Athena Scientific Belmont, MA, 1997.
- [4] Umberto Biccari, Yongcun Song, Xiaoming Yuan, and Enrique Zuazua. A two-stage numerical approach for the sparse initial source identification of a diffusion–advection equation. *Inverse Problems*, 39(9):095003, 2023.
- [5] Peter Borwein and Tamás Erdélyi. *Polynomials and polynomial inequalities*. Springer Science & Business Media, 2012.
- [6] Len Bos, Stefano De Marchi, Marco Vianello, and Yuan Xu. Bivariate lagrange interpolation at the padua points: the ideal theory approach. *Numerische Mathematik*, 108:43–57, 2007.
- [7] Marco Caliari, Stefano De Marchi, and Marco Vianello. Bivariate polynomial interpolation on the square at new nodal sets. *Applied Mathematics and Computation*, 165(2):261–274, 2005.
- [8] Eduardo Casas and Karl Kunisch. Using sparse control methods to identify sources in linear diffusion-convection equations. *Inverse problems*, 35(11):114002, 2019.
- [9] Antonin Chambolle and Thomas Pock. A first-order primal-dual algorithm for convex problems with applications to imaging. *Journal of Mathematical Imaging and Vision*, pages 120–145, 2011.
- [10] Shaobing Chen, David Donoho, and Michael A. Saunders. Atomic decomposition by basis pursuit. *SIAM Review*, pages 129–159, 2001.
- [11] Lenaic Chizat and Francis Bach. On the global convergence of gradient descent for over-parameterized models using optimal transport. *Advances in Neural Information Processing Systems*, 2018.
- [12] Javier Duoandikoetxea and Enrique Zuazua. Moments, masses de dirac et décomposition de fonctions. *CR Acad. Sci. Paris Sér. I Math*, pages 693–698, 1992.
- [13] Vincent Duval and Gabriel Peyré. Exact support recovery for sparse spikes deconvolution. *Foundations of Computational Mathematics*, pages 1315–1355, 2015.
- [14] Abdellatif El Badia, Tuong Ha-Duong, and Adel Hamdi. Identification of a point source in a linear advection–dispersion–reaction equation: application to a pollution source problem. *Inverse Problems*, 21(3):1121, 2005.
- [15] Heinz Werner Engl, Martin Hanke, and Andreas Neubauer. Regularization of inverse problems. *Mathematics and its Applications*, 375, 1996.
- [16] Stephen Fisher and Joseph Jerome. Spline solutions to  $l_1$  extremal problems in one and several variables. *Journal of Approximation Theory*, pages 73–83, 1975.
- [17] Roland Glowinski and Americo Marroco. Sur l’approximation, par éléments finis d’ordre un, et la résolution, par pénalisation-dualité d’une classe de problèmes de dirichlet non linéaires. *Revue française d’automatique, informatique, recherche opérationnelle. Analyse numérique*, pages 41–76, 1975.
- [18] Tom Goldstein and Stanley Osher. The split bregman method for  $l_1$ -regularized problems. *SIAM Journal on Imaging Sciences*, pages 323–343, 2009.
- [19] Leonid Hanin. An extension of the Kantorovich norm. In *Monge Ampère Equation: Applications to Geometry and Optimization (Deerfield Beach, FL, 1997)*, volume 226 of *Contemp. Math.*, pages 113–130. Amer. Math. Soc., Providence, RI, 1999.
- [20] Gongsheng Li et al. Determining magnitude of groundwater pollution sources by data compatibility analysis. *Inverse Problems in Science and Engineering*, 14(3):287–300, 2006.
- [21] Yingying Li, Stanley Osher, and Richard Tsai. Heat source identification based on constrained minimization. *Inverse Problems and Imaging*, 8(1):199–221, 2014.
- [22] Kang Liu and Enrique Zuazua. Representation and regression problems in neural networks: Relaxation, generalization, and numerics. *Mathematical Models and Methods in Applied Sciences*, 35(06):1471–1521, 2025.
- [23] Song Mei, Andrea Montanari, and Phan-Minh Nguyen. A mean field view of the landscape of two-layer neural networks. *Proceedings of the National Academy of Sciences*, 115(33):E7665–E7671, 2018.

- [24] Donald Newman and Harold Shapiro. Jackson's theorem in higher dimensions. In *On Approximation Theory*, pages 208–219. Springer, 1964.
- [25] Frank Olver et al. *NIST Handbook of Mathematical Functions*. Cambridge University Press, 2010.
- [26] Peter Olver. On multivariate interpolation. *Studies in Applied Mathematics*, 116(2):201–240, 2006.
- [27] Stanley Osher et al. An iterative regularization method for total variation-based image restoration. *Multiscale Modeling & Simulation*, pages 460–489, 2005.
- [28] Necat Ozisik. *Inverse heat transfer: fundamentals and applications*. Routledge, 2018.
- [29] Benedetto Piccoli and Francesco Rossi. On properties of the generalized wasserstein distance. *Archive for Rational Mechanics and Analysis*, 222:1339–1365, 2016.
- [30] Andrei Nikolaevich Tikhonov. On the solution of ill-posed problems and the method of regularization. In *Doklady akademii nauk*, volume 151, pages 501–504. Russian Academy of Sciences, 1963.
- [31] Michael Unser. A representer theorem for deep neural networks. *Journal of Machine Learning Research*, pages 1–30, 2019.
- [32] Michael Unser, Julien Fageot, and John Paul Ward. Splines are universal solutions of linear inverse problems with generalized TV regularization. *SIAM Review*, pages 769–793, 2017.
- [33] Cédric Villani. *Optimal transport: old and new*. Springer, 2009.